TIME-DEPENDENT BEHAVIOR OF MAHA SARAKHAM SALT AS AFFECTED BY CARNALLITE CONTENT

Naphaphat Wilalak

A Thesis Submitted in Partial Fulfillment of the Requirements for the

Degree of Master of Engineering in Geotechnology

Suranaree University of Technology

Academic Year 2016

พฤติกรรมที่ขึ้นกับเวลาของเกลือหินชุดมหาสารคามที่ได้รับผลกระทบจากปริมาณแร่คาร์นัลไลต์

นางสาวณภาภัช วิลาลักษณ์

วิทยานิพนธ์นี้เป็นส่วนหนึ่งของการศึกษาตามหลักสูตรปริญญาวิศวกรรมศาสตรมหาบัณฑิต
สาขาวิชาเทคโนโลยีธรณี
มหาวิทยาลัยเทคโนโลยีสุรนารี
ปีการศึกษา 2559

TIME-DEPENDENT BEHAVIOR OF MAHA SARAKHAM SALT

AS AFFECTED BY CARNALLITE CONTENT

Suranaree University of Technology has approved this thesis submitted in partial fulfillment of the requirements for the Degree of Doctor of Philosophy.

Thesis Examining Committee

_____

(Asst. Prof. Dr. Helmut Durrast)

Chairperson

_____

(Prof. Dr. Kittitep Fuenkajorn)

Member (Thesis Advisor)

_____

(Asst. Dr. Decho Phueakphum)

Member

_____   _____

(Prof. Dr. Sukit Limpijumnong)   (Assoc. Prof. Flt. Lt. Dr. Kontorn Chamniprasart)

Vice Rector for Academic Affairs   Dean of Institute of Engineering

and Innovation

ฉภาภัช วิลาลักษณ์ : พฤติกรรมที่ขึ้นกับเวลาของเกลือหินชุดมหาสารคามที่ได้รับผลกระทบจาก
ปริมาณแร่คาร์นัลไลต์ (TIME-DEPENDENT BEHAVIOR OF MAHA SARAKHAM SALT
AS AFFECTED BY CARNALLITE CONTENT) อาจารย์ที่ปรึกษา :
ผู้ช่วยศาสตราจารย์ ดร.เดโช เผือกภูมิ, 81 หน้า

        วัตถุประสงค์ของการศึกษาคือ เพื่อศึกษาผลกระทบของปริมาณแร่คาร์นัลไลต์ต่อพฤติกรรมการ
เปลี่ยนแปลงรูปร่างแบบทันทีทันใดและพฤติกรรมการคืบของเกลือหินจากแอ่งมหาสารคาม การทดสอบการ
คืบในแกนเดียวและในสามแกนได้ผันแปรปริมาณแร่คาร์นัลไลต์ตั้งแต่ร้อยละ 0 ถึง 90 โดยน้ำหนัก ภายใต้
ความเค้นกดเป็นระยะเวลา 21 วัน ผลการทดสอบ ได้นำมาสอบเทียบเพื่อหาค่าตัวแปรของพฤติกรรมเชิง
ยืดหยุ่น ความหนืดเชิงยืดหยุ่นและเชิงพลาสติกของแบบจำลอง Burgers ผลการสอบเทียบระบุว่าค่าตัวแปร
เชิงคณิตศาสตร์ในสมการ Burgers มีค่าลดลงแบบเอ็กซ์โพแนนเชียลเมื่อปริมาณแร่คาร์นัลไลต์เพิ่มขึ้น ได้มี
การสอบเทียบผลการทดสอบเพื่อหาค่าตัวแปรเชิงคณิตศาสตร์บนพื้นฐานของสมการการคืบแบบยกกำลัง ผล
ระบุว่าค่าตัวแปรเชิงคณิตศาสตร์มีค่าลดลงเมื่อปริมาณแร่คาร์นัลไลต์เพิ่มขึ้นเช่นกัน ผลกระทบของปริมาณ
และการกระจายตัวของแร่คาร์นัลไลต์ในตัวอย่างหิน ได้นำมาวิเคราะห์ด้วยแบบจำลองเชิงตัวเลขด้วย
โปรแกรม FLAC ผลการวิเคราะห์ระบุว่าที่ปริมาณแร่คาร์นัลไลต์เท่ากัน เมื่อมีการแทรกสลับของ
จำนวนชั้นของแร่คาร์นัลไลต์มากขึ้นส่งผลให้ค่าความหนืดเชิงพลาสติกมากขึ้นและค่าความเครียดเชิง
เวลามีค่าลดลง ผลการทดสอบได้นำมาคาดคะเนระยะเวลาของหลุมเจาะที่จะเกิดการเปลี่ยนแปลงรูปร่าง
และเกิดการพัง ผลระบุว่าระยะเวลาบริเวณที่เกิดการเปลี่ยนแปลงรูปร่างและเกิดการแตกมีค่าลดลงเมื่อ
ปริมาณแร่คาร์นัลไลต์เพิ่มขึ้นที่ระดับความลึกต่างๆ

สาขาวิชา เทคโนโลยีธรณี   ลายมือชื่อนักศึกษา _____
ปีการศึกษา 2559   ลายมือชื่ออาจารย์ที่ปรึกษา _____

NAPHAPHAT WILALAK : TIME–DEPENDENT BEHAVIOR OF MAHA

SARAKHAM SALT AS EFFECTED BY CARNALLITE CONTENT.

THESIS ADVISOR : ASST. PROF. DECHO PHUEAKPHUM, Ph.D., 81 PP.

CREEP/POTASH/SHAFT/BOREHOLE/SALT/CARNALLITE

The objective of this study is to experimentally determine the effects of carnallite contents on the instantaneous and time-dependent deformations of rock salt obtained from the Maha Sarakham formation. Uniaxial and triaxial creep tests have been performed on the specimens with carnallite contents varying from 0 to over 90 percent by weight. The test duration for the creep testing is 21 days. Regression analysis is performed on the test results to calibrate the elastic, visco-elastic and visco-plastic parameters. The Burgers parameters exponentially decrease with increasing the carnallite content ($C_\%$). For the potential laws the material parameters increase with increasing $C_\%$. The effects of the carnallite distribution in the specimens are analyzed by performing numerical simulations using FLAC code. The results indicate that under the same $C_\%$ the greater numbers of the inter-bedding between halite and carnallite induce higher visco-plastic coefficient, and hence results in a lower creep deformation. The result can predict the time at failure and dilation of borehole closure. The results indicate that the time at failure and dilation are decreases when carnallite content is increasing at different depth.

School of Geotechnology   Student's Signature———————

Academic Year 2016   Advisor's Signature———————

ACKNOWLEDGMENTS

I would like to express my sincere thanks to Prof. Dr. Kittitep Fuenkajorn for his valuable guidance and efficient supervision. I appreciate his strong support, encouragement, suggestions and comments during the research period. I also would like to express my gratitude to Asst. Prof. Dr. Decho Phueakphum and Dr. Prachya Tepnarong for their constructive advice, valuable suggestions and comments on my research works as thesis committee members. Grateful thanks are given to all staffs of Geomechanics Research Unit, Institute of Engineering who supported my work.

Finally, I would like to thank beloved parents for their love, support and encouragement.

Naphaphat Wilalak

TABLE OF CONTENTS

Page

TABLE OF CONTENTS (Continued)

TABLE OF CONTENTS (Continued)

TABLE OF CONTENTS (Continued)

Page

LIST OF TABLES

LIST OF FIGURES

LIST OF FIGURES (Continued)

SYMBOLS AND ABBREVIATIONS

ρ	=	Density of the specimen
ρ_s	=	Density of halite (2.16 g/cc)
ρ_c	=	Density of carnallite (1.60 g/cc)
γ_{oct}	=	Octahedral shear strains
τ_{oct}	=	Octahedral shear stress
t	=	Time
E_1	=	The elastic modulus
E_2	=	The spring constant in visco-elastic phase
η_1	=	Visco-plastic viscosity
η_2	=	Visco-elastic viscosity
$\varepsilon(t)$	=	Transient creep strain
σ	=	Stress
T	=	Absolute temperature
κ	=	Empirical constants
α	=	Empirical constants
β	=	Empirical constants
γ	=	Empirical constants
G	=	The shear modulus
K	=	The bulk modulus
E	=	The elastic modulus

SYMBOLS AND ABBREVIATIONS (Continued)

ν = The Poisson's ratio

T = Tensile strength

u_r = The radial displacement

P = The time-independent applied stress

A = The time-independent functions of position

B = The time-independent functions of position

r = Radius

a = Inner boundary

ε_r = Radial strain

$W_{d,f}$ = The distortional strain energy at failure

$W_{d,d}$ = The distortional strain energy at dilation

S_r = The radial stress deviation

σ_r = The radial stress

σ_θ = The tangential stress

σ_z = The vertical stress

σ^* = The equivalent (effective) stress

CHAPTER I

INTRODUCTION

1.1 Background and rationale

Inclusions and impurities in salt can affect its creep deformation and strength. The degree of impurity is different for different scales. Handin et al. (1984) state that natural rock salt may contain three forms of impurities: (1) extraneous minerals may be disseminated between halite grains, (2) some water may be trapped in the halite crystal structure or it may appear in brinefilled fluid inclusions or along grain boundaries; (3) foreign ions such as K^+, Ca^{2+}, Mg^{2+}, Br^- and I^- may be embedded in the crystal structure. The coupled effects of impurities on the mechanical properties of salt can be very complicated (Franssen and Spiers, 1990; Raj and Pharr, 1992; Senseny et al., 1992). Handin et al. (1984) compared the steady-state flow parameters obtained for pure halite with those for salt samples with 0.6% $MgCl_2$ inclusions and with 0.1% KCL inclusions, and conclude that the inclusions appreciably affect the creep rate of salt. The quantitative effect of these inclusions, however, cannot be determined due to insufficient data.

1.2 Research objectives

The objective of this study is to experimentally determine the effects of carnallite contents on the instantaneous and time-dependent deformations of rock salt obtained from the Maha Sarakham formation. Uniaxial and triaxial creep testing has

been performed on rectangular blocks of specimens obtained from a potash mine in the northeast of Thailand. The Burgers model and potential creep law are used to describe the elastic, visco-elastic and visco- plastic deformations of the specimens. Sets of empirical equations are derived to represent the variations of the material parameters with carnallite contents. Time-dependent closure equation of circular hole in an infinite plate is derived to predict the closure of ventilation borehole and service shaft in rock salt formation with varied carnallite contents. Finite difference analyses are performed to help explain the variations of the mechanical and rheological responses of the specimens with different carnallite contents.

1.3 Scope and limitations

1. All testing are conducted on rock salt specimens obtained from the Maha Sarakham formation (ASEAN Potash Mining Co., Ltd. (APMAC)).

2. Series of uniaxial and triaxial creep tests are performed with the applied axial stresses range from 2 to 31 MPa.

3. Uniaxial and triaxial creep tests are performed with confining pressures up to 7 MPa.

4. All creep tests are performed up to 21 days.

5. All tests are conducted under ambient temperature (25-28 °C).

6. The test procedures will follow the relevant ASTM standard practices.

7. All testing are made under dry condition.

8. The carnallite contents are varied from 0 to over 90 percent.

1.4   Research methodology

The research methodology shown in Figure 5 comprises 8 steps. Literature review is carried out to study the previous researches on time-dependent behavior of rock salt under unconfined and confined condition. Sample preparation and laboratory testing are performed under unconfined and confined. The testing results are used to develop mathematical relations of mathematical. Discussions are made to analyze the mechanical properties of creep testing and all research activities, methods, and results are documented and complied in the thesis.

1.4.1   Literature review

Literature review is carried out to study the previous researches on time-dependent behavior of rock salt by constant stress and confining pressure under unconfined and confined conditions. The sources of information are from text books, journals, technical reports and conference papers.

1.4.2   Sample collection and preparation

Rock salt samples have been donated by (ASEAN Potash Mining Co., Ltd. (APMC)) from the Khorat basin, northeast of Thailand. The salt cores belong to the Lower salt member of the Maha Sarakham formation (Warren, 1999). Samples are prepared for uniaxial and triaxial creep tests. The salt specimens are rectangular shape with nominal dimensions of $54 \times 54 \times 108$ mm^3 (L/D=2). Preparations of these samples will follow as much as practical the American Society for Testing and Materials (ASTM D7070-08). Over 20 specimens are used for this study.

```
┌─────────────────────────┐
│     Literature Review   │
└─────────────────────────┘
            │
            ▼
┌─────────────────────────┐
│    Sample Preparation   │
└─────────────────────────┘
            │
            ▼
┌─────────────────────────┐
│     Laboratory Tests    │
└─────────────────────────┘
```

| Uniaxial Creep Tests | | Triaxial Creep Tests |

Derivation of the Mathematical Relationships

Computer Simulations

Potential Applications

Discussions and Conclusions

Thesis Writing
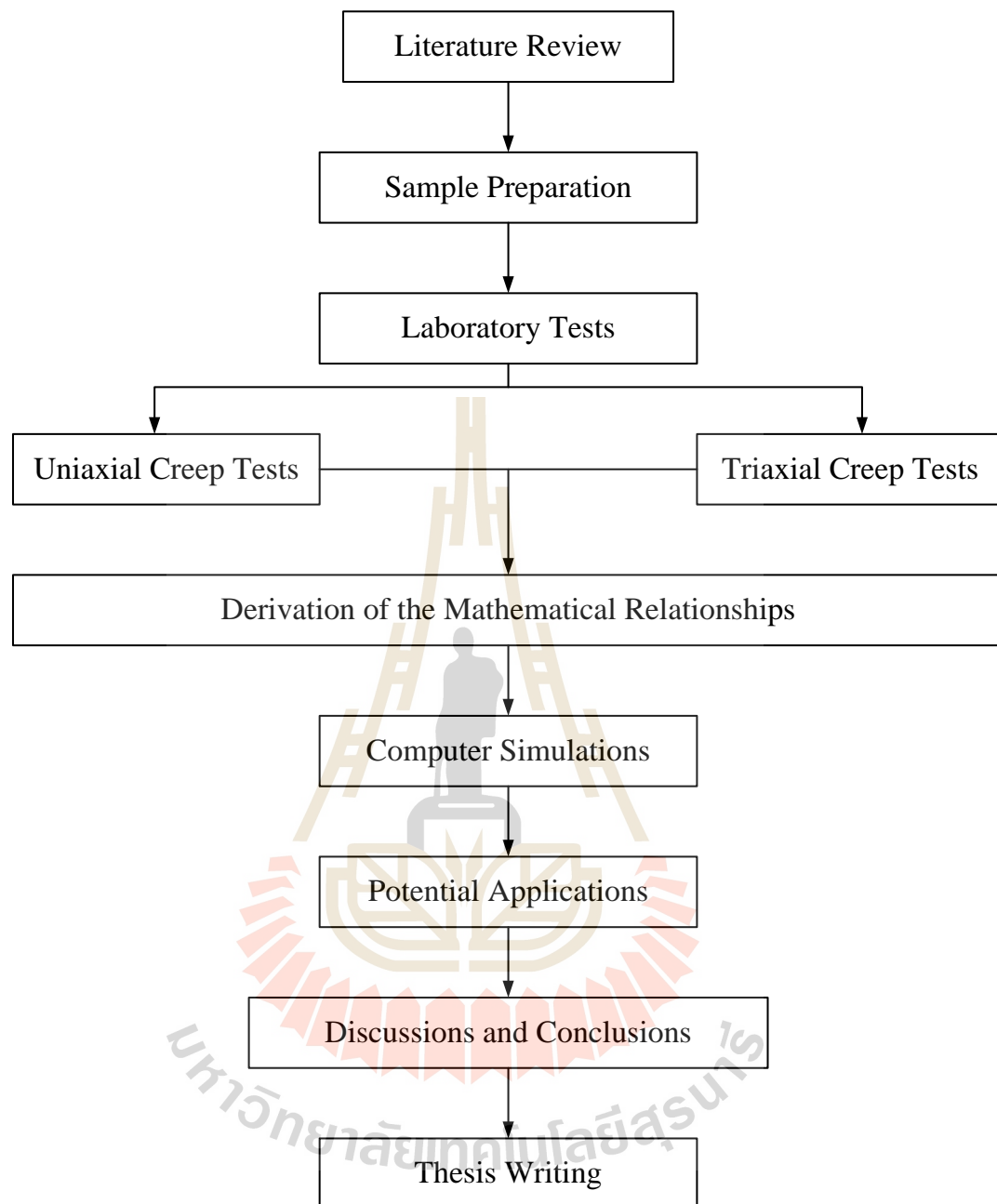
Figure 1.1 Research methodology.

1.4.3   Laboratory testing

Uniaxial and triaxial creep tests use about twenty specimens. A consolidation loading frame is used to apply constant axial stresses to the specimens. A polyaxial load frame is used to apply constant axial stresses and constant confined pressure to the specimens.

1.4.4   Mathematical relations

The Burgers parameters and potential creep law parameters are determined using the SPSS statistical software (Wendai, 2000) on the strain-time curves. The effects of carnallite content on these parameters are mathematically determined.

1.4.5   Computer simulations

A series of finite difference models is constructed to simulate the uniaxial creep test of rock salt specimens subjected to a constant axial stress. The carnallite inclusion in the specimen is defined as thin beds normal to the core axis. This is because all core specimens used in this research are obtained from vertically drilled holes. The non-linear time-dependent finite difference program, FLAC (Itasca, 1992) is used in the simulation.

1.4.6   Potential applications

The creep models calibrated from the strain-time curves of various carnallite contents is used to determine the time-dependent closure of boreholes in the potash mines. Governing equations for the borehole closure are derived. Usefulness of the research findings will be described.

1.4.7 Discussions and conclusion

The research finding is used to determine the time-dependent borehole closure. Discussions are made to reveal the reliability of the test data and the correctness of the interpretation and analysis.

1.4.8 Thesis writing

All research activities, methods, and results are documented and complied in the thesis.

1.5 Thesis contents

This research thesis is divided into eight chapters. The first chapter includes background and rationale, research objectives, scope and limitations and research methodology. The second chapter presents results of the literature review to improve an understanding of creep and behavior of salt and potash on case studies in Thailand and abroad. The Chapter three describes sample preparation. Creep test on laboratory described in chapter four. The empirical simulation calculation to predict the parameter using the Burgers model in chapter five. Chapter six used finite difference program, FLAC (Itasca, 1992) will be used in the simulation of specimen as a function of carnallite content. Application for determine the time-dependent closure of boreholes in the potash mines describes in chapter seven. Chapter eight presents discussions, conclusions and recommendation for future studies.

CHAPTER II

LITERATURE REVIEW

2.1 Introduction

This chapter summarizes the results of literature review carried out to improve an understanding of the time-dependent behavior of rock salt. The topics reviewed here include factors affecting rock salt behavior as affected by carnallite content.

2.2 Literature Review

2.2.1 Creep testing

2.2.1.1 Creep testing of rock salt

Researchers from the field of material sciences believe that rock salt behavior shows many similarities with that of various metals and ceramics (Munson and Wawersik, 1993; Chokski and Langdon, 1991). However, because alkali halides are ionic materials, there are some important differences in their behavior. Aubertin et al. (1992, 1993, 1998, 1999) conclude that the rock salt behavior should be brittle-to-ductile materials or elastic-plastic behavior. This also agrees with the finding by Fuenkajorn and Daemen (1988), Fokker (1995, 1998), and Fokker and Kenter (1994).

Jeremic (1994) discusses the mechanical characteristic of the salt behavior. They are divided into three characteristics: the elastic, the elastic-plastic, and the plastic behaviors. The elastic behavior of rock salt is assumed to be linearly elastic with brittle failure. The rock salt is observed as linear elastic only for a low magnitude of loading. The range of linear elastic mainly depends on the content of elastic strain

and can be used to formulate the modulus of elasticity. Normally, the modulus of elasticity of rock salt is relatively low. The elastic and plastic behavior of rock salt can be investigated from the rock salt specimen. The confined rock salt specimen at the beginning of incremental loading shows linear elastic deformation but with further load increases plastic behavior is induced, which continues until yield failure. Elastic deformation and plastic deformation are considered as separated modes of deformability in the great majority of cases. The salt material simultaneously exhibits both elastic strain and plastic strain. The difference between elastic behavior and plastic behavior is that elastic deformation is temporary (recoverable) and plastic deformation is permanent (irrecoverable). The degree of permanent deformation depends on the ratio of plastic strain to total strain. The elastic and plastic deformations can also be observed by short-term loading, but at higher load magnitude. The plastic behavior of rock salt does not occur if the applied stress is less than yield stress. The rock salt is deformed continually if the high stress rate is still applied and is more than the yield stress. Increasing the load to exceed the strain limit of the rock salt beyond its strength causes it to fail. The deformation of rock salt by the increase of temperature can also result in the transition of brittle-to-ductile behavior.

The time-dependent deformation (or creep) is the process at which the rock can continue deformation without changing stress. The creep strain seldom can be recovery fully when loads are removed, thus it is largely plastic deformation. Creep deformation occurs in three different phases, as shown in Figure 2.1, which relatively represents a model of salt properties undergoing creep deformation due to the sustained constant load. Upon application of a constant force on the rock salt, an instantaneous elastic strain (ε_e) is induced. The elastic strain is followed by a

primary or transient strain, shown as Region I. Region II, characterized by an almost constant slope in the diagram, corresponds to secondary or steady state creep. Tertiary or accelerating creep leading to rather sudden failure is shown in Region III. Laboratory investigations show that removal of applied load in Region I at point L will cause the strain to fall rapidly to the M level and then asymptotically back to zero at N. The distance LM is equal to the instantaneous strain ε_e. No permanent strain is induced here. If the removal of stress takes place in the steady-state phase the permanent strain (ε_p) will occur. From the stability point of view, salt structure deformations after constant load removal have only academic significance, since the stresses imposed underground due to mining operations are irreversible. The behaviour of the salts with time-dependent deformation under constant load is characterized as a visco-elastic and visco-plastic phenomenon. Under these conditions the strain criteria are superior to the strength criteria for design purposes, because failure of most salt pillars occurs during accelerated or tertiary phase of creep, due to the almost constant applied load.

The dimensions of a pillar in visco-elastic and visco-plastic rock should be established on the basis of a prediction of its long-term strain, to guard against adequate safety factor accelerating creep (Fuenkajorn and Daemen, 1988; Dusseault and Fordham, 1993; Jeremic, 1994; Knowles et al., 1998).

The Burgers model is one of linear visco - elastic models. These models yield a linear relationship between stress (σ) and strain rate ($\varepsilon(t)$ or $\partial\varepsilon/\partial t$) as follows:

$$\sigma + \left(\frac{\eta_1}{E_1} + \frac{\eta_2}{E_2} + \frac{\eta_1}{E_2}\right)\dot{\sigma} + \frac{\eta_1\eta_2}{E_1E_2}\ddot{\sigma} = \eta_1\dot{\varepsilon} + \frac{\eta_1\eta_2}{E_2}\ddot{\varepsilon} \qquad (2.1)$$
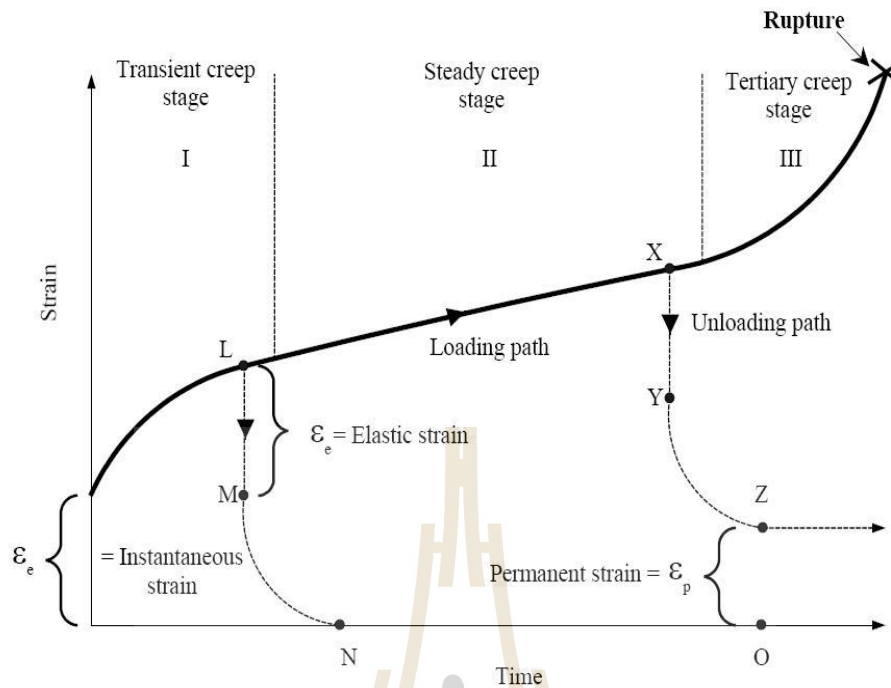
Figure 2.1 The typical deformation as a function of time of creep materials (modified from Jeremic, 1994).

The Burgers models describe equations for uniaxial constant stress, constant stress rate and constant rate testing. The derivation is made by using a Laplace transformation. For uniaxial constant stress, visco - elastic are presented as function of constant axial stress (σ_0), time and spring and dashpot constant shown in Figure 2.2 and equations as follows:

$$\varepsilon(t) = \sigma_0 \left\{ \frac{1}{E_1} + \frac{t}{\eta_1} + \frac{1}{E_2} \left[1 - \exp\left(- E_2 t / \eta_2 \right) \right] \right\} \tag{2.2}$$

Triaxial creep testing is conducted to determine the time-dependence of rock salt under confinements. The triaxial creep test is close to in-situ stress condition when applying confining pressures. Ong et al. (1998) study creep

deformation of salt and potash from Patience Lake Member. They perform the long-term triaxial creep tests. Adjustment of the desired axial and confining stress levels is quick. The axial and confining stress are maintained. The test can be a single stage test or multiple stage test which lasts for 90 days. The data storage interval at the start of a test is usually 5 minutes; it is changed to one hour when the creep rate decreased. Upon unloading, the sample is inspected, measured dimensionally. They are found that the salt is close to the plastic behavior under a high confining pressure.
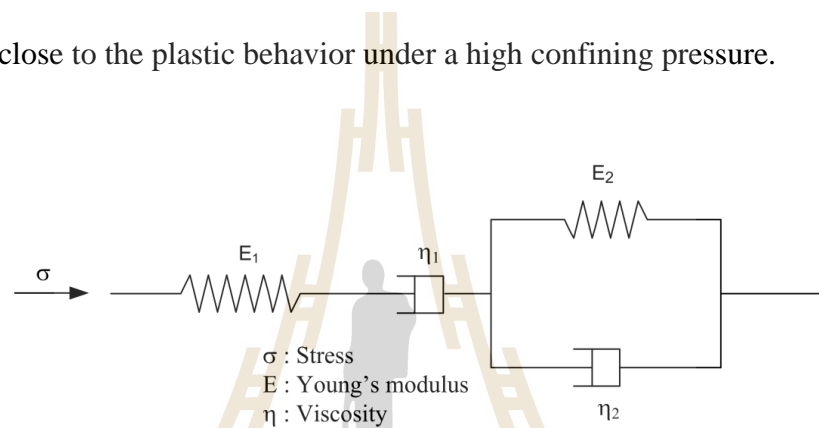
Figure 2.2 Burgers model built up of combinations of linear spring and dashpots (modified from Jeager and Cook, 2007).

Hamami et al. (1996) study the triaxial creep testing on salt. The triaxial creep test with low deviatoric stress under an axial stress varying between 5.5 and 15 MPa with a step of 2.5 MPa each 3 months. The triaxial creep test with constant deviatoric stress (under an axial stress of 13 MPa) and decreasing (and increasing) the temperature form 20 °C to 90 °C (and 90 °C to 20 °C) with a step of 10 °C each 1.5 months. They summarize the results that the temperature increase, as for the deviatoric stress, results in an increase of the material deformation. A decrease in temperature reduces remarkably the sample deformation, which is subjected to an important deformation at higher temperatures in the beginning of test. This phenomenon is strain

hardening. The strain rate depends on the stress, the temperature and the previous strain. This also agrees with the finding by Korthaus (1996).

Senseny (1984) studies the influence on creep of specimen size of salt for transient and steady–state deformation. Two specimen sizes, 10 mm and 50 mm diameter cylinders with a length to diameter ration of 3.0, were investigated by means of triaxial compression creep testing under various temperatures. The results were fitted to potential creep laws that steady –state creep does not. The rate of transient creep strain of the small specimens is higher than that of larger specimens. This implies that constitutive laws developed from laboratory data may over predict deformation measured in the field, especially if the formulation results largely from transient creep.

Fokker (1998) studies that effect of grain size on the creep behavior and strength of the rock salt and field condition. The average grain size of the salt visually observed from the core and post failure specimens were 5mm x 10mm x 12 10mm. It was concluded that the large size of the salt crystals increases the effect of the crystallographic features on the mechanics of deformation and failure of the samples.

Study by Franssen and Spiers (1990), Raj and Pharr (1992) and Senseny et al. (1992) concludes that the shear strength and deformation of halite crystals are orientation dependent. The small size of the sample may not provide good representative test results. This also reflects on the specifications by ASTM (ASTM D2664-95a, D2938-95 and D3967-95a). The ASTM standard methods specify that to minimize the effect of grain size the sample diameter should be at least ten times the average grain size.

Inclusions and impurities in salt have an effect on to the creep deformation and strength of salt. The degree of impurity is varying for different scales of the rock salt. On a small scale, such as for laboratory specimens, the impurities of salt involve ferruginous inclusions and thin clay seams along grain boundaries or bedding planes. The impurities distribute uniformly in the salt may affect the strength of rock salt. This can decrease the creep deformation and strength of rock salt. These phenomena have been reported by Franssen and Spiers (1990), Raj and Pharr (1992) and Senseny et al. (1992), as well.

Bonding between grains can affect the creep rate and the strength of salt. The bonding between the crystals is weak in rock salt. Allemandou and Dusseault (1996) observe the post –failure from the Brazilian strength test and uniaxial compressive strength tests. They report that stress depends on the boundary between grains and crystals.

Bachu et al. (2005) propose the salt characteristics and behavior of the Middle Devonian Elk Point Group in the Alberta basin in western Canada, these salt beds are found at depth that range from several hundred meters to more than 2000 meter. The salt beds range in thickness from several tens to a few hundred meters. The vertical stress (weight of the overburden) at the top of these salt beds ranges from 10 to 50 MPa, and temperatures vary between 20 and 70°C. Stresses are assumed to be isotropic and equal to the lithostatic (overburden) within the salt beds, because salt visco plastic properties and slow creep tend to dissipate shear stresses. Vertical stress gradients at the top and bottom of the salt beds are in the 24–25 kPa/m range, and differ by only 0.1–0.3 kPa/m between the two, indicating that they are basically constant across the entire rock package containing the salt beds. If a salt cavern is filled with a

14

fluid at an initial pressure, in the long term the pressure inside the cavern will change as a result of any of: (1) salt creep, (2) leakage along the well bore, (3) thermal expansion of the cavern fluid, (4) flow of the fluid out of the cavern into the adjacent strata, or (5) additional salt solution or precipitation in the cavern (Berest et al., 2000).

Weidinger et al. (1997) conduct research in deep underground salt for the host material for the permanent storage of radioactive and toxic wastes. Dimensioning and safety analysis of such repositories require a model which allows to predict the creep behavior of rock salt on the basis of the microstructure and the physical mechanisms of deformation. Already before testing natural rock salt contains a subgrain structure. During deformation under constant stress the creep rate changes until a steady state is reached. The same holds for the microstructural parameters subgrain size and spacing of dislocations inside subgrains. The composite model of plastic deformation takes the observed heterogeneity of the dislocation structure explicitly into account. Using this model in combination with appropriate kinetic laws for dislocation movement, transient as well as steady-state creep of rock salt can be calculated. In conclusion it can be stated that the composite model of plastic deformation allows to calculate transient as well as steady-state creep behavior of rock salt on the basis of the observed microstructure and deformation mechanisms with physically reasonable values for the model parameters. Therefore, the thermomechanical behavior of rock salt around a permanent repository for radioactive and toxic wastes can be predicted for long periods of time with high reliability

Zhang et al. (2012) evaluate the effect of the long-term operation of a salt cavern in a given construction on rock deformation and its stability, tri-axial creep tests to the glauberite, anhydrite, and argillaceous rock salt are conducted, from

which the creep curves as well as exponential functions of strain rate during the steady creep stage and creep constitutive equations of different rock salt in the experimental process derived are obtained. The study results under the same deviatoric stress, the strain rate of argillaceous rock salt is lower than the glauberite and anhydrite, and the difference becomes larger with the increase of the deviatoric stress.

Table 2.1 The creep parameters of different rock salt (modified from Zhang et al., 2012).

Type	σ_1 (MPa)	K (GPa)	G_0 (GPa)	G_1 (GPa)	η_1 (GPa·h)	η_2 (GPa·h)
Glauberite rock salt	22.01	14.65	8.09	97.23	180.56	7309
	28.28	17.95	9.66	107.68	399.42	6779
	36.17	18.59	8.95	35.34	516.81	3158
	42.43	14.65	7.20	26.39	210.78	1492
Anhydrite rock salt	33.95	27.55	22.00	213.60	310.11	4781
	39.96	26.22	19.93	67.26	478.70	3346
	46.20	26.50	11.99	23.94	155.08	2331
	52.15	18.86	8.41	21.94	326.41	1379
Argillaceous rock salt	28.10	31.69	22.41	95.61	153.82	10476
	39.98	32.58	20.80	180.53	1660.80	13563
	46.18	31.40	18.91	215.48	3455.00	12468
	51.96	29.58	17.72	147.98	1662.90	10859

The creep constitutive equations of different kinds of rock salt are in good agreement with the Burgers model, besides which the respective characteristics of these two creep models are compared. The change of creep parameters also illustrates the discrepancy of rock salt. The researching results can provide some references for long-term stability analysis of gas storage in salt caverns. The Burgers model parameters of different rock

salt, which are obtained by the matlab program and based on the experiment data and methods in references (Wang and Li, 2007; Shen and Xu, 1997) are listed in Table 2.1.

Yang et al. (1999) study the confining pressure effects on the time-dependent stress strain behavior of salt rock. The steady-state creep strain rate increases as deviatoric stress increases but decreases as confining pressure increases. An exponential function is suggested to model the creep strain from transient to steady-state and found fitting well the creep strain. Calculated values using the proposed functions are compared with experimental results. The relationship between the steady-state creep strain rate and confining pressure can be approximated by an exponential function. The relationship between the steady-state creep strain rate and deviatoric stress can be approximated by a power function.

Yahya et al. (2000) show how a unified model with a single set of equations and material constants can be used for describing inelastic flow of rock salt submitted to a variety of loading conditions associated with plasticity, creep and relaxation. After introducing the complete model in its full expanded version, the authors demonstrate that these different observed material responses are specific manifestations of a unique (unified) inelastic behavior, each corresponding to an imposed load path. The unified model relies on the use of internal state variables (ISV) attached to specific phenomena, including isotropic and kinematic hardening. Each ISV appears in the kinetic (flow) law and evolves according to a growth rule as a function of the inelastic strain tensor until it reaches saturation. The flow law, which relates the deviatoric stress to the inelastic strain rate, takes into account the evolution of these ISV as well as the external (observable) variables. Together, they represent a complete description of inelastic flow. These concepts are illustrated by results obtained on rock

salt samples submitted to different loading conditions, including constant strain rate (CSR) tests, creep (constant stress) tests, and relaxation (constant strain) tests. As a single set of parameters is able to describe these different types of test results, which are usually associated to plasticity, creep and relaxation, it can be concluded that the inelastic behavior of rock salt, like that of other crystalline materials, exhibits a unique (unified) inelastic behavior that can be represented by a single kinematic law with accompanying evolution laws for the ISV. This means that there is no need to develop separate expressions for pseudo-inviscid plasticity, long term creep, and distinct relaxation behavior, as these are simply different manifestations of a unique inelastic behavior for specific load paths.

2.2.1.2 Creep testing of carnallite

Suwanich (2007) studies the potash-evaporite deposits in the northeastern portion of Thailand. The northeastern Thailand forms as the landscape of low elevation plateau (about 150-220 m. above mean sea level). This is called Khorat plateau. The Khorat plateau is divided into 2 basins, the north basin or Sakhon Nakhon basin and the south basin or Khorat basin. The potash minerals are deposited in the Maha Sarakham Formation which is the rock salt main deposits. The Maha Sarakham Formation is consisted of 3-layer salt beds, the Upper, Middle and Lower salt layers. These salt beds are interbedded by clastic sediments of sticky reddish brown mainly clay. The potash minerals have been found only at the top of the Lower Salt. There are only 2 kinds, carnallite ($KMgCl_3 \cdot 6H_2O$) and sylvite (KCl). They are usually deposited and interlocking with halite or rock salt grains and called the carnallitite and sylvite strata. The other evaporate minerals mostly found in the potash minerals are tachyhydrite (Mg-rich mineral) and rare boracites and gypsum. The structure of the

Maha Sarakham Formation varies from common salt strata to salt domes. The Lower

Salt in domed up through the Middle and Upper Salt closing to the surface. The peak

or highest point of the domes is leached by groundwater remaining only the salt whereas

the flank around the domes still remains the potash mineral containing sylvinite mainly.

The carnallite is usually found beyond the flank of the domes. The theory said that the

carnallite is the primary mineral while the sylvite is the secondary deposit altered from

carnallite reacting with the groundwater in suitable condition.

Mellegard et al. (2012) investigates the mechanical properties of

potash in the laboratory. The test specimens contained varying amounts of sylvite and

carnallite. The use of X-Ray Diffraction (XRD) are costly and required destruction of

the post-test sample. An alternative approach was to use the mineralogical assay result

obtained by the mining company through use the X-Ray Fluorescence (XRF). Analysis

of the laboratory testing data include sorting the test result into two separate databases,

one for halite and one for sylvite. Initially, the shorting of the data was bases on the

bulk density of each specimen that was calculated during the specimen fabrication

process. The density of halite is reported as 2.16 g/cc, while the density of sylvite is

reported as 1.99 g/cc. Therefore, low-density specimens assumed to be high in either

sylvite or carnallite, were categorized as having a density that ranged from 1.99 to 2.11

g/cc. High-density assumed to be high in halite content, were categorized as having a

density that ranged from 2.12 to 2.19 g/cc.

Weck et al. (2014) reported density functional calculations of the

structures and properties of carnallite ($KCl \cdot MgCl_2 \cdot 6H_2O$) possesses the orthorhombic

space group *Pnna*, with Z = 12, and computed lattice parameters: a = 16:28 Å, b = 22:83

Å, c = 9:59 Å; $\alpha = \beta = \gamma = 90°$ (V = 3564.13 Å^3; b/a = 1:40; c/a = 0:59). The crystal

structure of carnallite consists of a network of face-sharing KCl_6 octahedra and of isolated $Mg\cdot(H_2O)_6$ octahedra occupying the openings in the KCl network, with the water molecules acting as charge transmitters between Mg^{2+} and Cl^- ions. The computed interatomic distances are 2.06-2.09 Å for $Mg-OH_2$ and 3.18-3.36 Å for K-Cl forming octahedra and the HCl hydrogen bonds are predicted to be in the range 2.14-2.19 Å. The computed structure is about 3.0% larger than the structure characterized by Schlemper and co-workers (Schlemper et al., 1985) using XRD (Table 2.2), with good agreement found between calculated and measured axial ratios (i.e. b/a = 1:394; c/a = 0:592). The measured interatomic distances in the octahedra are 2.027-2.053 Å for $Mg-OH_2$ and 3.154-3.321 Å for K-Cl and the experimental H-Cl hydrogen bonds are in the range 2.255-2.429 Å.

Table 2.2 Crystallographic data calculated at the GGA/PBE level of theory Hawthorne and Ferguson, 1975).

Name Sp. gp. Z	Carnallite *Pnna* 12
a (Å)	16.28
b (Å)	22.83
c (Å)	9.59

King (1972) performs creep tests on model pillars of Saskatchewan potash ore. The first series of tests show the effect to changes in temperature and vertical stress on the creep behavior of pillars in a homogeneous material. In the second series are incorporated the effects of the presence of clay seams in the roof and floor. The test conditions in both series of tests represent those existing at subsurface depths of between 3400 and 4500 ft. in Saskatchewan. For the first series

of tests with a pillar diameter to height ratio of 4 the vertical natural strain on the pillars cloud be related to the time by a simple power law. Thus the rate of vertical creep of the model pillars was found that a pillars diameter to height ratio of at least 8 was required to prevent brittle failure at vertical stress equivalent to depths of 3400 ft. With this diameter to height ratio of 8 the creep behavior for tests equivalent to this depths was very similar to that of pillars in a homogeneous material at the same depth, but having a diameter to height ratio of 4.

Duncan et al. (1993) conduct creep tests on the Esterhazy- and the Patience-Lake-types of potash salt rocks from Saskatchewan, Canada are presented. The investigations involved over 6 years of time-dependent experiments in uniaxial compression using potash from the Rocanville and the Lanigan mines of the Potash Corporation of Saskatchewan. A creep test at a given load would last from 2 to 8 months, with most tests conducted over a 4 month period. Since the yield stress of both types of potash lies between 9 and 11 MPa, there is very little creep below 11 MPa. Between 11 and 13 MPa, creep strain production increases sharply through plastic deformation. Above about 13 MPa, however, plastic creep is dominated by brittle creep caused by micro cracking. As a result, the lateral and volume creep strain curves may then display the transient and the steady-state, or all three stages of creep, while the axial strain, which is not affected by micro cracking, usually attenuates for the whole duration. Two different interpretations of the results are offered. Identifying the last (the fourth) month of testing with the steady-state model, the stress dependence of the steady-state rate has been established for both rock types. The alternate interpretation proceeds on the assumption that under 13 MPa, both the axial and the lateral strain can be modelled through the power function formulation of transient strain.

2.2.2 Potential creep law

Lindner and Brady (1984), Langer (1984), and Farmer (1983) present numerous empirical equations describing the time - dependent behavior of geological materials. Two types of empirical laws that explicitly contain creep strain, stress, and time variables are selected for use this investigation: potential laws (Nair and boresi, 1970; Horseman and Passaris, 1984; Harrington, 1980; Starfield and McClain, 1973; Nair et al., 1974) and exponential laws (Langer, 1984). The laws are applied to describe salt behavior without considering the actual mechanism of deformation. Generally, empirical constitutive model are developed by linking the creep strain to stress and temperature. The potential laws are power equations relating creep strain, stress, time and temperature. Two empirical models describing transient and steady – state creep strains can be expressed as:

$$\varepsilon(t) = K' \sigma^{\beta} t^{\gamma} T^{\alpha} \quad \text{(transient)} \tag{2.3}$$

$$\dot{\varepsilon}(t) = A' \sigma^{B} T^{C} \quad \text{(steady – state)} \tag{2.4}$$

The exponential laws present the transient creep strain as a function of stress, time and temperature in exponential form:

$$\varepsilon(t) = B' \sigma^{m} t^{n} \exp(-\lambda / T) \tag{2.5}$$

Where $\varepsilon(t)$ is transient creep strain, $\dot{\varepsilon}(t)$ is steady – state creep strain rate, σ is stress, t is time, T is absolute temperature, K′, α, β, γ, A′, B, C, B′, m, n, λ is empirical constants.

These constitutive equations (Equation 2.3 and 2.4) give the creep strain as a function of stress history, time and empirical constants for a one-dimensional problem. Three-dimensional analysis can be developed from each equation individually by using the visco-plasticity flow rule (Harrington, 1980). The time-dependent strain induced in salt consists of both transient and steady state components. Combining these two constitutive equations for use in three-dimensional analysis is difficult. The methods used to determine the time at which the steady-state creep strain is established remain inconclusive. For short-term predictions (i.e. less than one year), 46 both models give similar results. The prediction can be significantly different for long-term periods (Lindner and Brady, 1984).

2.3   Numerical Method

FLAC (Itasca, 1992a, 1992b) is a two-dimensional explicit finite difference program for engineering mechanics computation. This program simulates the behavior of structures built of soil, rock or other materials that may undergo plastic flow when their yield limits are reached. Materials are represented by elements, or zones, which form a grid that is adjusted by the user to fit the shape of the object to be modeled. Each element behaves according to a prescribed linear or nonlinear stress/strain law in response to the applied forces or boundary restraints. The material can yield and flow and the grid can deform (in large-strain mode) and move with the material that is represented. The explicit, Lagrangian calculation scheme and the mixed-discretization

zoning technique used in FLAC ensure that plastic collapse and flow are modeled very accurately. Because no matrices are formed, large two-dimensional calculations can be made without excessive memory requirements. The drawbacks of the explicit formulation (i.e., small time step limitation and the question of required damping) are overcome to some extent by automatic inertia scaling and automatic damping that do not influence the mode of failure. Contamination of rock salt is the important factor that caused the variance. Make strength is increased or decreased so depending on kind of ore in rock salt. We can be used program computer describe intrinsic variability of the rock salt as effect by carnallite content. Though FLAC was originally developed for geotechnical and mining engineers, the program offers a wide range of capabilities to solve complex problems in mechanics. Several built-in constitutive models are available that permit the simulation of highly nonlinear, irreversible response representative of geologic, or similar, materials.

Fahimifar et al. (2010) study in the effect of creep, in the response of the tunnel. The objective is to predict time dependent displacement of the tunnel wall, after stopping the excavation or after installing the support system. The rock mass is assumed to be isotropic and homogenous and incompressible. The tunnel is assumed to be circular and driven in a hydrostatic stress field. The rate of excavation is considered to be infinitely large. The Burger's body which is able to model the primary and secondary creep regions of the rock mass is applied. In such a condition, an analytical solution for predicting time-dependent deformation of tunnel wall is derived. Thereafter, the application of the proposed solution is illustrated through three examples. So three example discussed consider a circular unlined tunnel in a hydrostatic stress field under far and near section from the face of the tunnel. The results presented suggest that there

exists a close agreement between the analytical solution and the numerical solution (Flac) for far and near section , but there exists a different between two analyses for the sections which have an approximate distance less than one time of the tunnel radius from the tunnel face.

Fuenkajorn (2007) studies the intrinsic variability of rock salt. The steady-state creep phase, the dislocation climb mechanism will dominate the deformation of salt specimens containing large crystals, resulting in a higher visco-plasticity. A series of finite element mesh models were constructed to simulate the uniaxial creep test of rock salt specimens subjected to a constant axial stress. The anhydrite inclusion in the specimen of rock salt was defined as thin beds normal to the core axis. The non-linear time-dependent finite element program, GEO (Fuenkajorn and Serata, 1994; Stormont and Fuenkajorn, 1994) was used in the simulation. Table 2.3 lists the material property parameters used in the computer simulations.

The visco-plastic coefficients of salt specimens increase exponentially with the crystal size, as the dislocation glide mechanism dominates the creep deformation for the specimens containing large salt crystals. On the other hand, pure salt specimens with fine crystals are deformed mostly by the dislocation climb mechanism, resulting in a lower visco-plasticity. Results from computer simulations suggest that the amount and number of anhydrite layers can reduce the creep strain in the steady-state phase, and hence increase the visco-plasticity of the salt specimens. The clay mineral content of less than 5% (the highest found in the salt tested) seems to have an insignificant impact on the salt mechanical properties of salt. The effect of clay content beyond 5% remains unclear.

Chen et al. (2006) conduct a numerical investigation of heat and moisture transfer in a bed of porous polycrystalline potash pellets. In this study a non-equilibrium mathematical model of temperature and moisture distribution within the bed was developed. Simulations were performed for a bed of potash pellets that is subjected to flows of humid air on the upper boundary and a cold impermeable surface on the lower boundary. The numerical predictions are in good agreement with the experiments and within the experimental uncertainty bounds. The model predicts that beds of porous potash pellets will contain less moisture than other types of potash fertilizer beds that are exposed to the same environmental conditions. The predictions also indicate that most of the accumulated moisture will be located in the top 10% of the bed and that the pore space relative humidity will be much greater than the supply air relative humidity.

Table 2.3 Material property parameters used in the computer simulations (Wetchasat, 2002; Jandakaew, 2003).

	Parameters	**Halite**	**Anhydrite**
Elastic	Elastic Modulus (E), GPa	2.48	150
	Poisson's Ratio (n)	0.20	0.18
	Shear Modulus (G_1), GPa	10.3	69.0
	Bulk Modulus (K_1), GPa	13.8	82.8
Visco-Elastic	Retard Shear Modulus (G2), GPa	6.90	69.0
	Retard Bulk Modulus (K2), GPa	20.7	82.8
	Visco-elastic Viscosity (V2), GPa	9.0	55.2
Visco-Plastic	Visco-platic Viscosity (V4), GPa	17.2	55.2

Chen et al. (2006) conduct a numerical investigation of heat and moisture transfer in a bed of porous polycrystalline potash pellets. In this study a non-equilibrium mathematical model of temperature and moisture distribution within the bed was

developed. Simulations were performed for a bed of potash pellets that is subjected to flows of humid air on the upper boundary and a cold impermeable surface on the lower boundary. The numerical predictions are in good agreement with the experiments and within the experimental uncertainty bounds. The model predicts that beds of porous potash pellets will contain less moisture than other types of potash fertilizer beds that are exposed to the same environmental conditions. The predictions also indicate that most of the accumulated moisture will be located in the top 10% of the bed and that the pore space relative humidity will be much greater than the supply air relative humidity.

2.4   Borehole Closure

Munteanu and Cristescu (2000) studied the variation of stress during creep convergence of a deep borehole excavated in rock salt is examined. A non-associated elasto/viscoplastic constitutive equation is used to describe both compressibility and/or dilatancy during transient and steady-state creep, as well as evolutive damage possibly leading to failure. An in-house FEM numerical method is used for this purpose. The conclusions for displacement and stress distribution around a borehole excavated in rock salt are compared: the elastic solution (E), the simplified solution assuming stress constancy during creep (S), and a numerical solution (N) taking into account the stress variation during creep closure of the borehole. It is shown that at relative small depth, and ratio of far field stress n=1, the solutions S and N are quite close and thus the first estimation of the borehole convergence can be obtained with a very simple formula. At greater depths and for n≠1 a numerical solution (N) which makes no simplifying assumption is needed. Also, it is shown that in long time intervals a sudden failure is

possible due to the slow variation of the stresses. This problem will farther be investigated.

CHAPTER III

SAMPLE PREPARATION

3.1 Introduction

This chapter describes sample preparation and specifications of the tested rock salt specimens. The method follows as much as practical the standard practices. The tested samples have been obtained from underground openings of ASEAN Potash Mining Co., Ltd. (APMC). They belong to the Lower Salt member of the Maha Sarakham formation. Warren (1999) describes the origin and geological structures of the Maha Sarakham salt. The samples contain mixture between halite and carnallite. They are sometimes called carnallitite. An attempt to obtain cylindrical cores has been made in the laboratory. During drilling the cores with high carnallite content tended to break along the bedding planes, particularly at the interfaces between the carnallite and halite. The specimens used for uniaxial creep tests are therefore prepared as rectangular blocks with nominal dimensions of $54 \times 54 \times 108$ mm^3. A high speed rock cutting device is used. Organic oil is used as cutting fluid. Figure 3.1 shows some examples of the rectangular block specimens with various carnallite contents. Chemical analyses by X-ray diffraction (XRD) performed on some specimens show that the primary mineral compositions of the specimens are halite and carnallite, which are of interest in this study (Table 3.1). Due to the difference of the densities between halite and carnallite, the carnallite content ($C_\%$) for each specimen can be determined by the following relation:

$$C_\% = \left(\frac{\rho_s - \rho}{\rho_s - \rho_c} \right) \times 100 \tag{3.1}$$

where ρ is density of the specimen, ρ_s is density of halite (2.16 g/cc) and ρ_c is density of carnallite (1.60 g/cc) (Klein et al., 1998). Table 3.2 shows the density and the C% of the specimens.
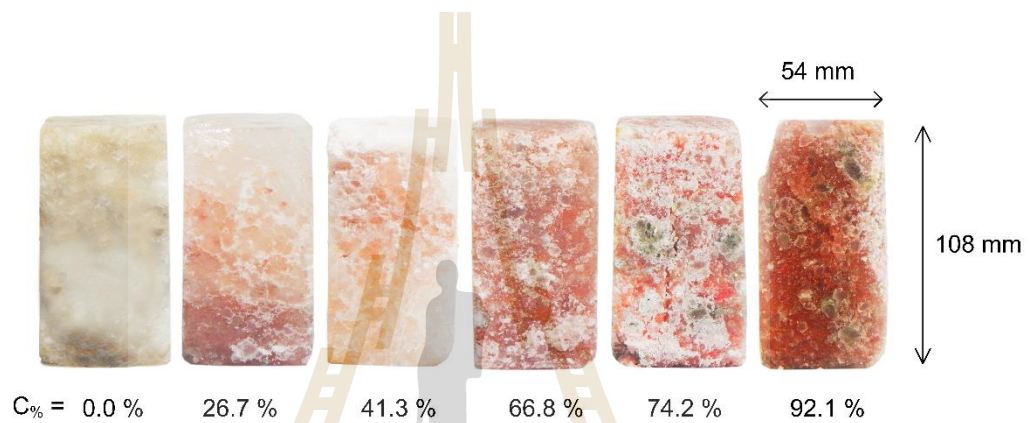
Figure 3.1 Some specimens prepared for creep testing.

Table 3.1 Chemical compositions of some specimens.

Components	Sample (1)	Sample (2)	Sample (3)	Sample (4)
Carnallite ($KMgCl_3\ 6H_2O$)	0.05	24.75	38.31	52.98
Halite (NaCl)	92.40	64.60	42.80	35.97
$MgCl_2$	5.71	8.93	9.69	5.55
Calcite ($CaCO_3$)	0	0.21	0.48	1.92
Anhydrite ($CaSO_4$)	0.11	0.17	0.65	1.23
Sylvite (KCl)	0.09	0.19	6.10	1.01
Hydrophilite ($CaCl_2$)	0	0	1.64	0.56
Wuestite	0	0.06	0.43	0.44
Calcium Chloride (CaCl)	1.65	1.08	0.89	0.33
Density (g/cc)	2.11	1.96	1.89	1.76
$C_\%$ (determined by density ratio)	8.56	36.12	49.01	71.08

Table 3.2 Specimen dimensions prepared for creep test.

Specimens No.	Width (mm)	Length (mm)	High (mm)	Weight (g)	Density (g/cc)	C%
Creep-01	52.02	52.27	108.60	574.40	1.94	38.43
Creep-02	54.92	54.75	108.80	604.20	1.85	55.95
Creep-03	54.97	55.25	109.60	594.40	1.79	66.87
Creep-04	54.35	54.87	108.62	567.10	1.75	73.13
Creep-05	53.92	54.77	109.27	552.70	1.71	79.93
Creep-06	53.70	54.15	110.20	564.10	1.76	71.36
Creep-07	55.75	57.00	113.22	668.80	1.86	53.78
Creep-08	55.67	57.15	113.70	722.70	2.00	28.99
Creep-09	54.10	54.57	108.05	555.30	1.74	74.88
Creep-10	54.95	56.02	109.42	595.50	1.77	70.05
Creep-11	55.72	55.50	109.15	577.30	1.71	80.33
Creep-12	54.15	54.05	109.37	624.10	1.95	37.57
Creep-13	53.30	52.90	105.30	503.50	1.70	82.88
Creep-14	55.30	55.55	109.85	554.90	1.64	92.07
Creep-15	54.92	55.30	109.92	550.60	1.65	91.23
Creep-16	54.32	54.95	109.32	555.10	1.70	81.98
Creep-17	52.90	52.85	99.65	525.30	1.89	49.02
Creep-18	54.85	54.57	108.92	605.60	1.86	54.05
Creep-19	54.70	54.37	108.55	614.20	1.90	46.01
Creep-20	45.97	46.20	89.62	355.50	1.86	52.24

Table 3.2 Specimen dimensions prepared for creep test (continued).

Specimens No.	Width (mm)	Length (mm)	High (mm)	Weight (g)	Density (g/cc)	$C_\%$
Creep-21	46.35	45.87	90.35	323.20	1.68	85.29
Creep-22	45.50	45.05	92.12	307.60	1.62	94.83
Creep-23	55.10	54.90	107.65	541.30	1.66	88.88
Creep-24	51.95	55.17	110.32	577.20	1.82	59.78
Creep-25	55.12	54.37	109.72	547.50	1.66	88.45
Creep-26	54.77	55.15	110.00	618.50	1.86	53.34
Creep-27	53.95	53.85	109.42	652.40	2.05	19.25
Creep-28	54.17	54.42	109.00	665.60	2.07	15.88
Creep-29	54.12	54.87	109.45	665.60	2.04	20.09
Creep-30	53.80	53.75	108.17	560.00	1.79	66.04
Creep-31	53.70	53.57	108.52	531.60	1.70	81.67
Creep-32	54.70	54.60	107.40	534.00	1.66	88.43
Creep-33	54.42	54.70	109.95	594.20	1.81	61.55
Creep-34	53.55	54.00	110.68	626.50	1.96	36.15
Creep-35	55.71	55.83	109.25	577.40	1.70	82.27
Creep-36	54.25	54.05	107.90	547.70	1.73	76.59
Creep-37	54.85	54.75	108.83	584.40	1.79	66.39
Creep-38	61.70	61.70	149.60	951.00	2.13	5.86
Creep-39	58.65	53.13	108.65	701.88	2.07	15.48
Creep-40	62.40	62.40	120.90	749.00	2.03	23.78

Table 3.2 Specimen dimensions prepared for creep test (continued).

Specimens No.	Width (mm)	Length (mm)	High (mm)	Weight (g)	Density (g/cc)	$C_\%$
Creep-41	52.80	54.35	108.05	642.00	2.07	15.98
Creep-42	54.00	55.60	112.18	714.83	2.12	6.70
Creep-43	55.45	55.33	108.43	635.60	1.91	44.49
Creep-44	54.33	55.73	109.55	544.60	1.64	92.47
Creep-45	63.10	63.10	138.00	915.00	2.12	6.90
Creep-46	54.39	54.41	108.40	600.30	1.87	51.56
Creep-47	54.75	54.00	109.50	607.50	1.88	50.62
Creep-48	53.00	54.38	109.00	617.00	1.96	34.97
Creep-49	56.75	54.75	109.38	651.90	1.92	43.16
Creep-50	54.88	56.25	109.63	589.80	1.74	74.46

CHAPTER IV

CREEP TESING

4.1 Introduction

The objective of the laboratory testing is to determine the effects of carnallite on time-dependent properties of the Maha Sarakham rock salt. This chapter describes the method.

4.2 Uniaxial and triaxial creep test

The polyaxial load frame has been used to apply constant axial stress (σ1) and lateral stresses (σ_2 and σ_3) on the triaxial creep test shown in figure 4.1 and a consolidation load frame (Jandakaew, 2007) has been used to apply constant axial stress for uniaxial creep test (Figure 4.2). It has been used in this study because the cantilever beam with pre-calibrated dead weight can apply a truly constant axial stress to specimens. Pre-calculated dead weight loading devices are used to apply constant axial loads to the specimens. Except the specimen shape the test procedure follows, as much as practical, the American Society for Testing and Materials (e.g. ASTM D7070-08). Neoprene sheets are placed at the interfaces between the loading platens and specimen surfaces. Each specimen is tested up to 21 days. The axial deformation is monitored using displacement digital gages. They are used to calculate the axial strains of the specimen. The readings are made every one minute for the first hour. After that the reading interval are gradually increased to every hour. The specimens are tested under the axial stresses of 2 to 31 MPa. Uniaxial triaxial creep test will be performed with

confining pressure up to 7 MPa. The three low stresses are selected for high C% specimens while the high values are for pure halite specimens. Note that the uniaxial compressive strength of pure halite is about 30 MPa (Sriapai et al., 2012).
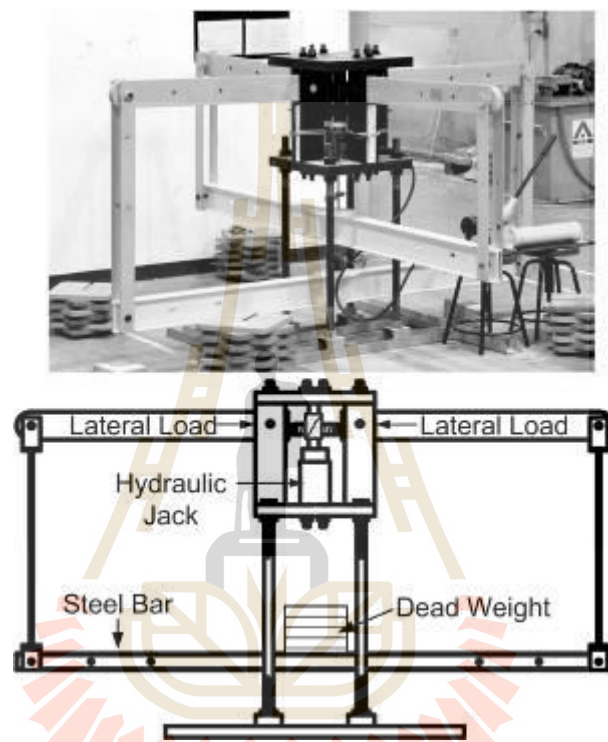
Figure 4.1 Polyaxial load frame (Fuenkajorn and Phueakphum, 2010).
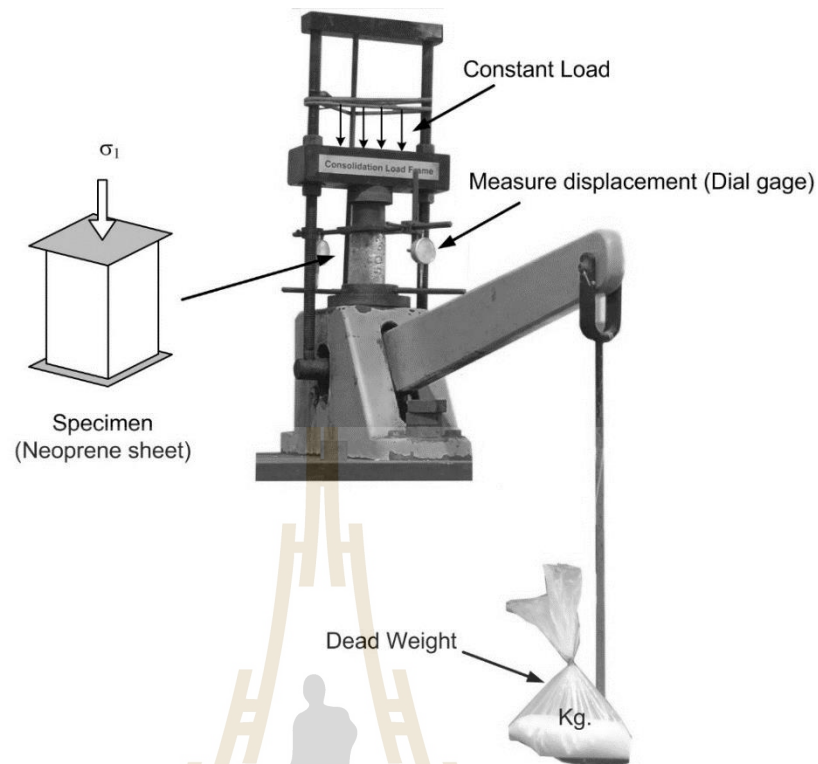
Figure 4.2 Consolidation load frame for the uniaxial creep.

4.3   Test results

Figure 4.3 shows the axial strain-time curves as a function of time for all tested specimens. The curves show the instantaneous, transient and steady-state creep phases of the rock salt. Larger creep strains are obtained for the specimens with high carnallite contents (Figure 4.3.). The creep deformation for the pure halite specimens agrees well with those of (Fuenkajorn, 2007) who performs creep testing on the same salt. Some specimens, particularly with high carnallite content and under high axial load, fail prior to the defined 21 days testing period.

For the triaxial creep test, the axial (vertical) constant stresses are from 12, 30 to 31 MPa, and the confining pressures range from 3, 7 to 7.2 MPa. Four specimens

have been tested up to 21 days. Figure 4.4 shows the principal strains (ε_1, $\varepsilon_2 = \varepsilon_3$) as a function of time for all specimens. For all loading conditions the axial strains (ε_1) increase with the carnallite contents and the applied stresses. Similar to those of the uniaxial creep results the instantaneous, transient and steady-state deformations can be clearly observed. Higher carnallite contents induce larger instantaneous and creep strains.
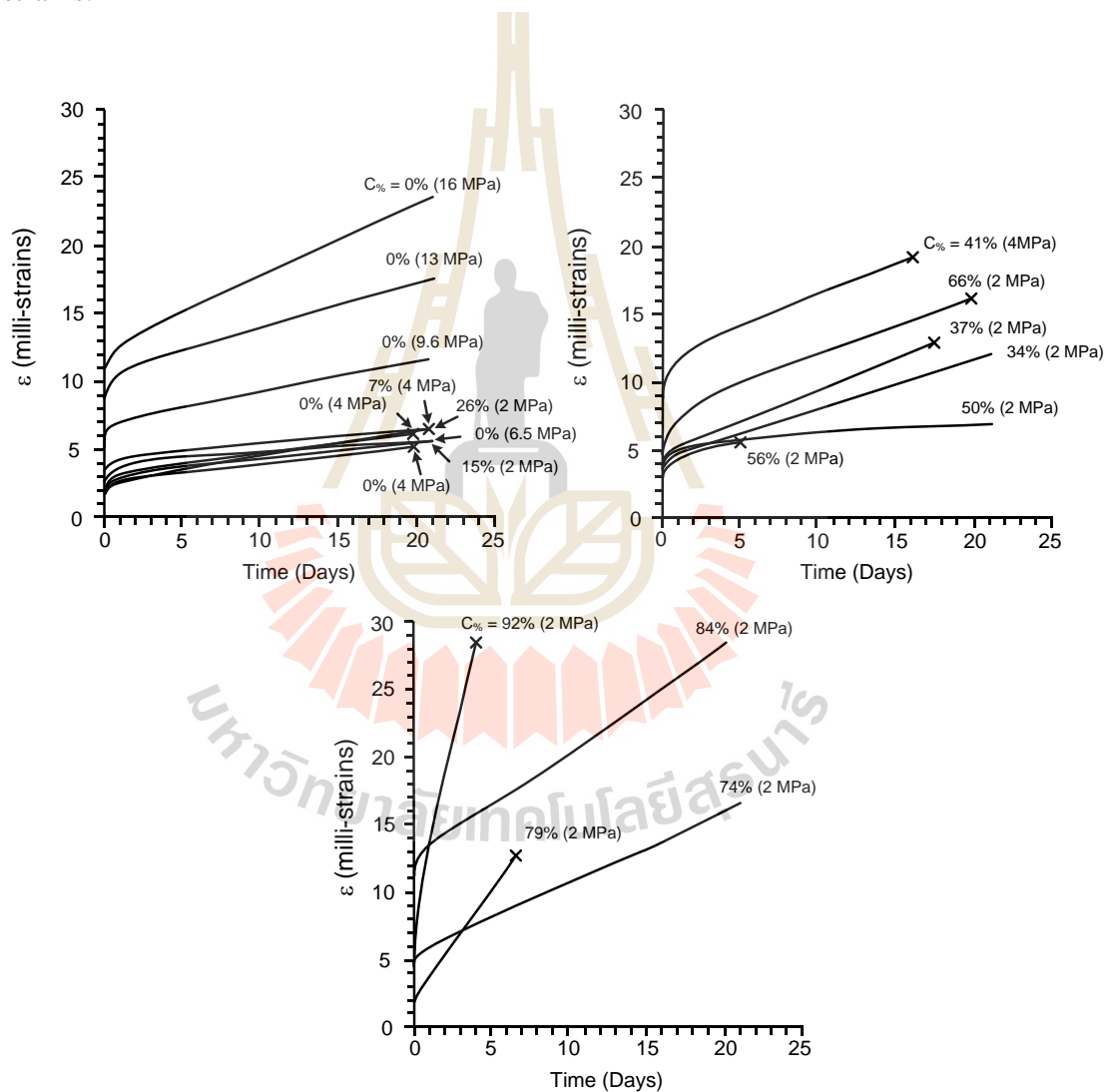
Figure 4.3 Uniaxial strain-time curves, numbers in bracket indicate constant axial stress.
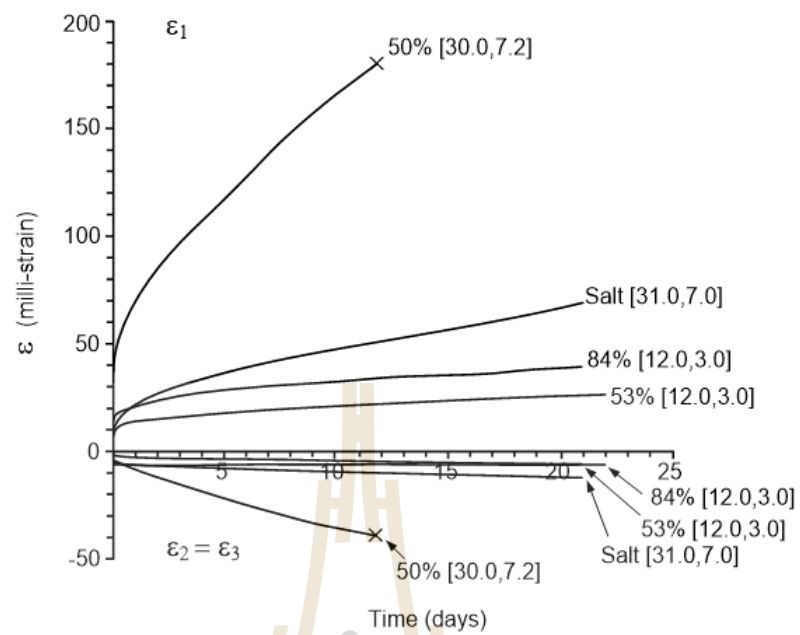
Figure 4.4 Axial and lateral strain-time curves for triaxial creep testing, numbers in

bracket indicate constant applied stresses [σ_1 ,σ_3] (Jandakaew, 2007).

CHAPTER V

CREEP PARAMETERS

5.1 Introduction

The purpose of this chapter is to calibrate the test results with the Burgers model and potential creep law. The effort is to help explain the effect of the carnallite contents on the creep behavior of the specimens.

5.2 Burgers Model

The Burgers model (Richard 1993) is used to describe the time-dependent deformation of the creep test specimens. It is recognized that numerous creep models or constitutive equations have been developed to represent the time-dependent behavior of rock salt (e.g., Gnirk and Johnson 1964; Handin et al. 1984; Langer 1984; Hardy and Sun 1986; Senseny et al. 1992). The Burgers model is used because it is simple and capable of describing the elastic, visco-elastic and visco-plastic phases of deformation. The governing equation for uniaxial and triaxial creep test under constant deviatoric stresses and confining pressure can be developed and presents the time-dependent octahedral shear strains (γ_{oct}) as a function of time and octahedral shear stress (τ_{oct}) as follows (Richard 1993):

$$\gamma_{oct}(t) = \tau_{oct}[(t/\eta_1) + (1/E_1) + (1/E_2) \cdot (1 - \exp(E_2 \cdot t/\eta_2))] \tag{5.1}$$

where t is the testing time, E_1 is the elastic modulus, E_2 is the spring constant in visco-elastic phase, η_1 is the viscosity coefficient in steady-state phase, and η_2 is the viscosity coefficient in transient phase. Figure 5.1 shows the physical components arranged in the Burgers model.
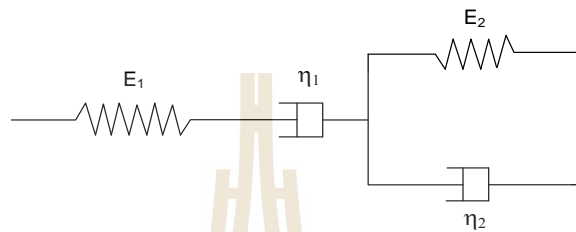
Figure 5.1 Modular components of Burgers model.

Regression analyses on the strain-time curves based on Equation (5.1) using the SPSS statistical software (Wendai, 2000) can determine the Burgers parameters for each specimen. Table 5.1 summarizes the calibration results. It is found that exponential equations can adequately describe the decreases of E_1, E_2, η_1 and η_2 as $C_\%$ increases (Figure 5.2):

$$E_1 = 2.330 \exp \cdot (-0.021 \cdot C_\%) \qquad \text{GPa} \qquad (5.2)$$

$$E_2 = 2.164 \exp \cdot (-0.018 \cdot C_\%) \qquad \text{GPa} \qquad (5.3)$$

$$\eta_1 = 42.413 \exp \cdot (-0.037 \cdot C_\%) \qquad \text{GPa·day} \qquad (5.4)$$

$$\eta_2 = 1.353 \exp \cdot (-0.026 \cdot C_\%) \qquad \text{GPa·day} \qquad (5.5)$$

All equations provide fairly good correlations with the test data, with R^2 greater than 0.8. Relatively high variations of the calibrated Burgers parameters are observed. This could be explained by the complex mechanical responses of the two different materials (halite and carnallite) within the specimen. As $C_\%$ approaches 100% the parameters E_1 and E_2 become very low, suggesting that pure carnallite tends to behave as the Maxwell material or viscous material with very low elasticity. This is also supported by the low elastic moduli of the specimens for $C_\%$ approaching 100%, obtained by the uniaxial compression test reported earlier.
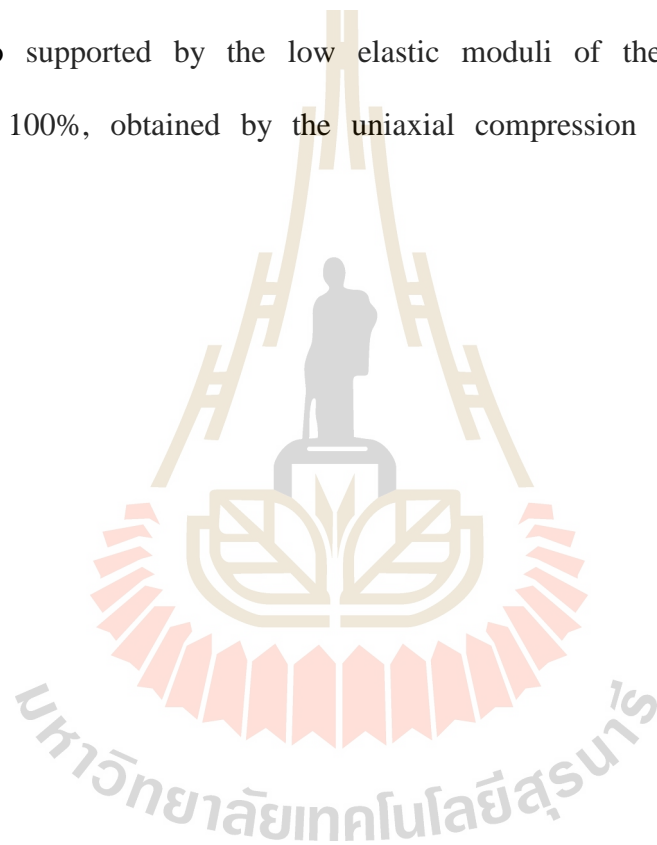
Table 5.1 Calibration of the Burgers parameters.

Carnallite contents (%)	Applied τ_{oct} (MPa)	Burgers Parameters			
		E_1 (GPa)	E_2 (GPa)	η_1 (GPa·Day)	η_2 (GPa·Day)
0	1.9	2.1	2.3	51.2	2.7
0	1.9	2.7	2.2	27.4	1.3
0	3.1	2.7	2.7	180.6	2.8
0	4.5	3.2	2.2	47.1	1.7
0	6.1	3.7	1.7	42.6	1.0
0	7.5	2.8	2.2	32.0	1.0
0	10.7	1.7	1.5	26.92	2.1
7.1	1.9	3.1	1.9	27.5	0.9
15.9	0.9	2.1	1.2	13.8	0.5
26.7	0.9	0.6	1.6	20.2	0.2
34.9	0.9	0.6	1.6	5.5	0.2
37.6	0.9	0.8	1.0	4.1	0.3
41.3	1.9	0.5	1.0	8.9	0.4
50.0	10.7	0.8	1.1	18.0	1.1
50.6	0.9	0.5	1.4	22.6	0.7
53.0	4.2	0.9	0.5	1.7	0.3
56.0	0.9	0.9	1.3	6.3	0.2
66.8	0.9	0.6	0.4	4.8	0.3
74.2	0.9	0.4	0.6	5.0	0.2
79.9	0.9	0.8	1.0	1.6	0.1
84.0	4.2	0.9	0.3	2.6	0.4
84.8	0.9	0.2	0.5	3.3	0.2
92.1	0.9	0.5	0.4	0.4	0.1
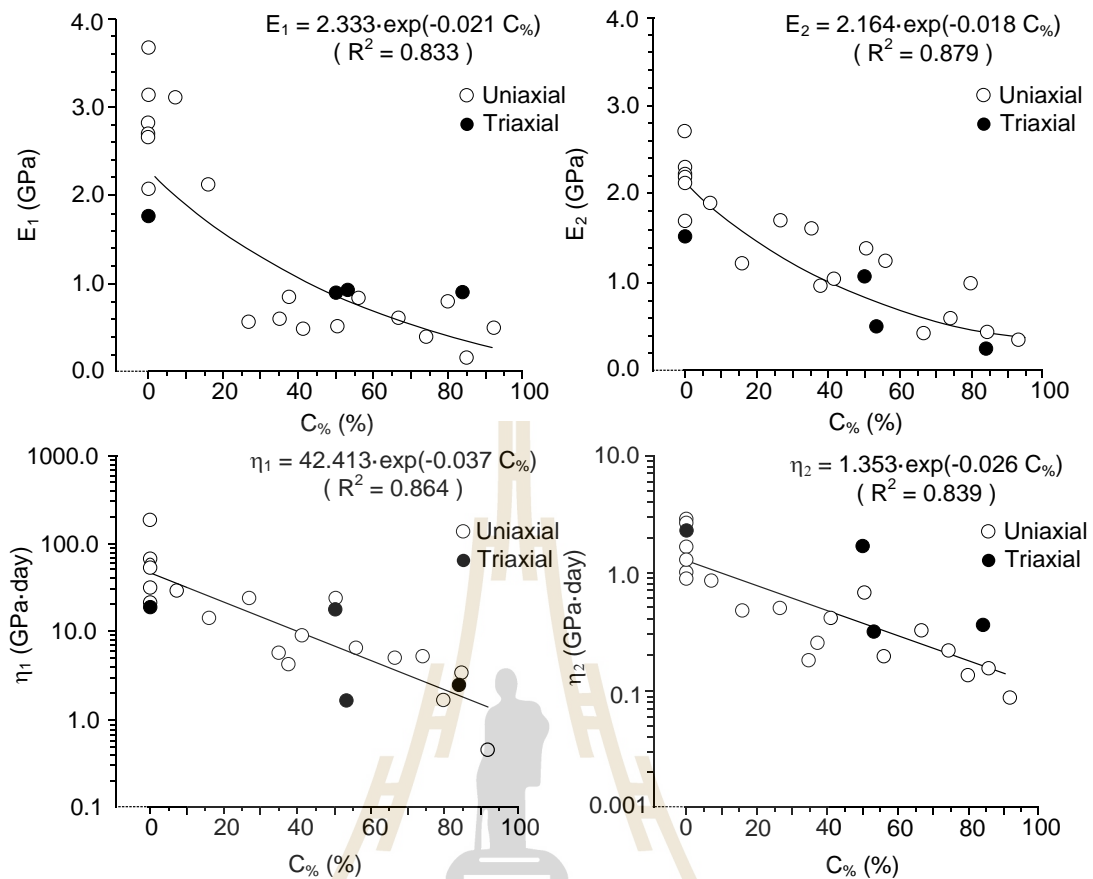
Figure 5.2 Burgers model parameters as a function of carnallite content.

5.3 Potential laws

The potential law is applied to describe salt behavior without considering the actual mechanism of deformation. Generally, empirical constitutive model is developed by linking the creep strain to stress time under isothermal condition. The potential law is power equation relating creep strain, stress and time. For this approach, the elastic strain (time-independent strain) is calculated by the classical elastic theory. The empirical models describing transient and steady-state creep strains can be expressed as:

$$\epsilon(t) = \kappa \cdot \sigma^{\beta} \cdot t^{\gamma} \cdot T^{\alpha} \qquad \text{(transient)} \qquad (5.6)$$

where $\epsilon(t)$ is transient creep strain, σ is stress, t is time, T is absolute temperature, κ, α, β, γ is empirical constants. Regression analyses on the strain-time curves based on Equation (5.6) using the SPSS statistical software (Wendai, 2000) can determine the potential parameters for each specimen under isothermal condition. Table 5.2 summarizes the calibration results. It is found that exponential equations can adequately describe the decreases of κ, β, γ and E as C% increases (Figure 5.3):

$$\kappa = 0.0003 \exp \cdot (0.0255 \cdot C_{\%}) \qquad 1/\,(\text{MPa·day}) \qquad (5.7)$$

$$\beta = 1.3589 \exp \cdot (0.0005 \cdot C_{\%}) \qquad (5.8)$$

$$\gamma = 0.1941 \exp \cdot (0.003 \cdot C_{\%}) \qquad (5.9)$$

$$E = 3.743 \exp \cdot (-0.022 \cdot C_{\%}) \qquad \text{GPa} \qquad (5.10)$$

All equations provide fairly good correlations with the test data, with R^2 greater than 0.8. The time-dependent parameters from the uniaxial creep and triaxial creep tests results showing creep parameters increase when carnallite content increases.

Table 5.2 Calibration of the potential parameters.

Carnallite contents (%)	Applied τ_{oct} (MPa)	Potential Parameters		
		κ (1/MPa·day)	β	γ
0.0	1.9	0.0003	1.5	0.2
0.0	1.9	0.0003	1.5	0.2
0.0	3.1	0.0002	1.4	0.2
0.0	4.5	0.0002	1.4	0.2
0.0	6.1	0.0002	1.4	0.2
0.0	7.5	0.0001	1.6	0.2
0.0	10.7	0.0006	1.0	0.2
7.1	1.9	0.0003	1.3	0.2
15.9	0.9	0.0006	1.5	0.2
26.7	0.9	0.0009	1.4	0.2
34.9	0.9	0.0011	1.5	0.2
37.6	0.9	0.0010	1.4	0.2
41.3	1.9	0.0010	1.4	0.2
50.0	10.7	0.0013	1.2	0.3
50.6	0.9	0.0013	1.0	0.2
53.0	4.2	0.0005	1.3	0.2
56.0	0.9	0.0011	1.3	0.2
66.8	0.9	0.0015	1.6	0.3
74.2	0.9	0.0020	1.7	0.2
79.0	0.9	0.0020	1.3	0.3
84.0	4.2	0.0020	1.1	0.3
84.8	0.9	0.0024	1.7	0.2
92.0	0.9	0.0030	1.6	0.3
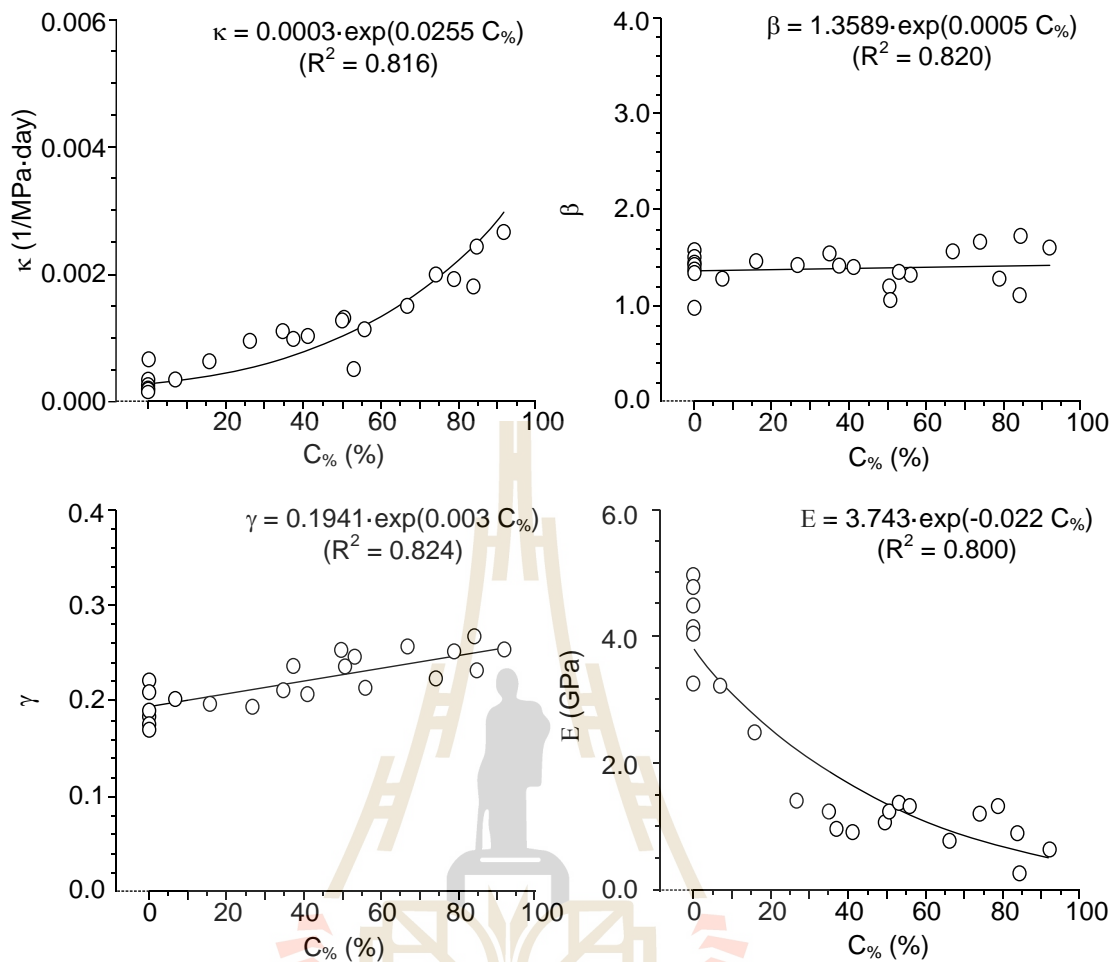
Figure 5.3 Potential parameters as a function of carnallite content.

5.4 Discussions

The test results fit fairly well to the Burgers model as suggested by the high values of the correlation coefficient (Figure 5.2). The Burgers parameters from the creep tests compared reasonably well with those of Fuenkajorn et al. (1988). The first spring, E_1 the combination of E_2 and η_2 , and the first dashpot η_1 represent instantaneous response, transient behavior and steady state behavior, respectively. The correlation coefficients seem high compared to other linear viscoelastic models, primarily due to the larger number of fitting parameters. For creep testing, elasticity

of the first spring varies from 5.0 to 2.0 GPa. The second spring seems to be more consistent. The dashpot viscosities, η_1 vary significantly, by about two orders of magnitude. The variation of the instantaneous elastic modulus, E_1 is mainly due to the nonlinear relationship between stress and strain. The parameter increases with decreasing stress level. Since there is no correlation between the stress level and the parameters E_2, η_1 and η_2 the scattering of these parameters might be caused by variation of intrinsic properties of the specimens. When $C_\%$ approaches 100%, E_1 and E_2 becomes very low approaching zero. This suggests that the pure carnallite specimen is likely to behave as viscous material with very low elasticity.

For the potential laws the material parameters increase with increasing $C_\%$. The parameter κ is highly sensitive to $C_\%$. The parameter β tends to be insensitive to $C_\%$. Note that both Burgers model and potential law are equally good and can adequately represent the creep behavior of the specimens under various carnallite contents.

CHAPTER VI

COMPUTER SIMULATIONS

6.1   Introduction

This chapter describes the results of finite difference analyses using FLAC (Itasca, 1992) to demonstrate the impact of carnallite content on the variability of the creep deformation of the salt specimen. The time-dependent parameters calibrated from the uniaxial creep tests are used in the computer simulation.

6.2   Numerical simulations

FLAC (Itasca, 1992) is a two-dimensional explicit finite difference for describing the time-dependent and intrinsic variability of the rock salt as affected by carnallite content. It is used to simulate because the explicit Lagrangian calculation scheme and the mixed-discretization zoning technique used in FLAC ensure that plastic collapse and flow can be modeled accurately. Several built-in constitutive models are available that permit the simulation of highly nonlinear, irreversible response representative of geologic, or similar, materials.

An attempt is made here to assess the impact of the amount and distribution of the carnallite on the time-dependent deformation of the specimens used in the uniaxial creep testing. Owing to the presence of two symmetry planes, only one-fourth of the specimen is modelled and analyzed (Figure 6.1).
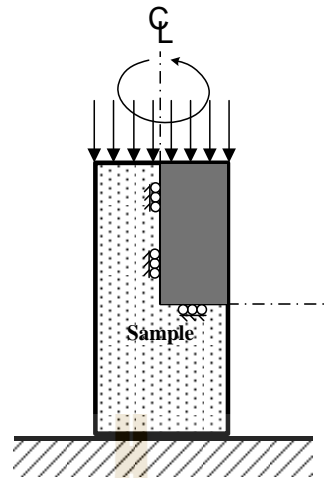
Figure 6.1 One-fourth of the specimen used in the axis-symmetry analysis.

The finite difference code (FLAC-Itasca 1992) is used in the simulations. Specimen models have a length-to-diameter ratio of 2.0. Series of finite difference models are constructed to simulate the specimens under constant uniaxial stresses (Figure 6.2). The carnallite content in the specimen models is defined as thin layers normal to the core axis. The models are classified into four groups with different $C_\%$'s: 20, 40, 60 and 80% by volume. Each group has different numbers of carnallite layers: 1, 3, 5 and 7. The analysis is made in axial symmetry. The left side of the model represents the centerline which does not allow horizontal displacement. The bottom boundary represents the mid-height of the specimen and does not allow vertical displacement. The right side of the mesh model is unconfined and can move freely in both directions.

Table 6.1 lists the material property parameters for pure halite and pure carnallite used in the computer simulations. The Poisson's ratio and tensile strength are obtained from Luangthip et al. (2016). The shear modulus and bulk modulus can be calculated as follow:

$$G = E/ 2 \cdot (1 + \nu) \tag{6.1}$$

$$K = E/ 3 \cdot (1 - 2\nu) \tag{6.2}$$

The top of the model is subjected to a uniform and constant axial stress of 2 MPa. The localized shear stresses induced in the specimens with different amount and distribution of carnallite are shown in Figures 6.3 to Figure 6.6. They are concentrated at the interfaces between the halite and carnallite layers.

The larger number of layers shows more concentration of the shear stresses. Figure 6.7 shows the simulated axial strain–time curves. Larger strains and strain rates are obtained for the specimens with higher $C_\%$. The presence of carnallite layers notably reduces the strain rates in the steady-state creep phase. Under the same $C_\%$, increasing the number of carnallite layers further reduces the strain rates. This is because the additional carnallite layers increase the number of interfaces between the carnallite and halite, and hence increases the localized shear stress locations which enhances the lateral resistance within the specimens.
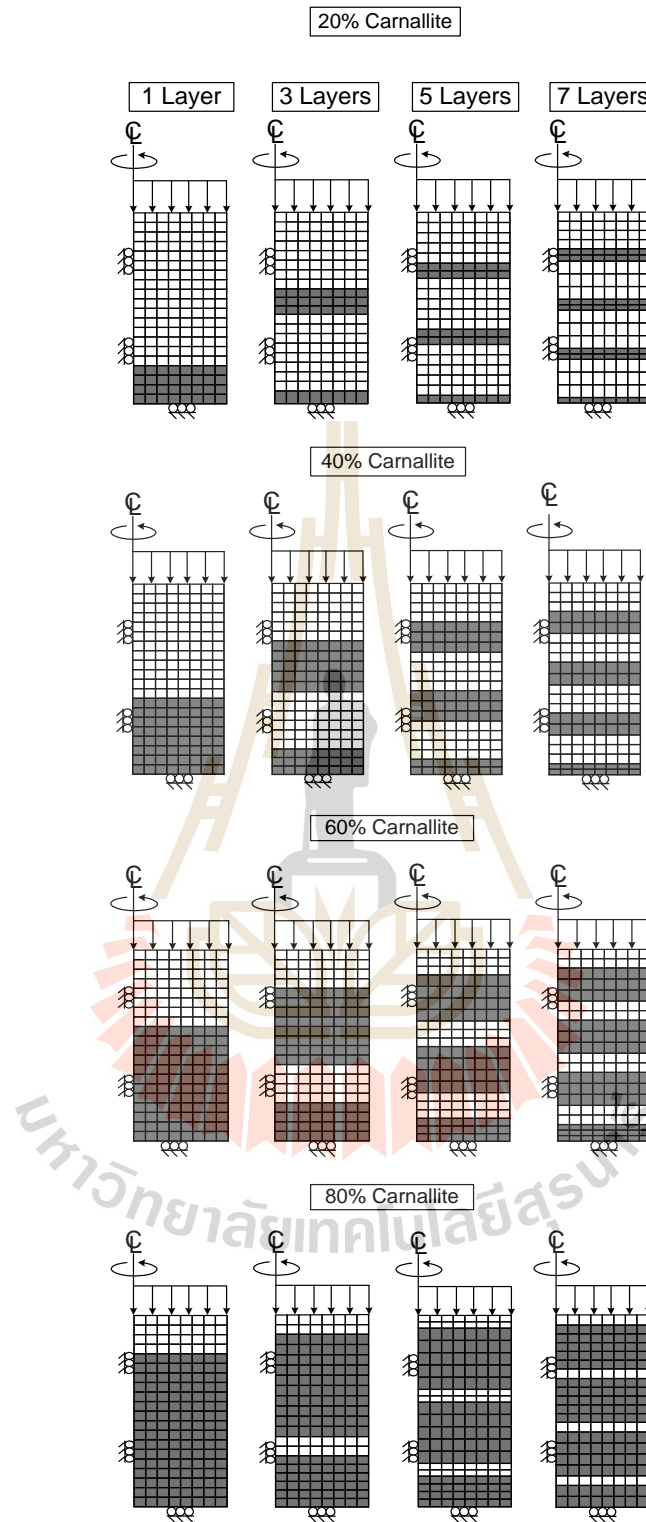
Figure 6.2 Mesh models of uniaxial creep test specimens with various amounts and distributions of carnallite (shaded areas).

Table 6.1 Material property parameters used in the FLAC.

Parameters	Pure halite	Pure carnallite
Elastic modulus (E_1, GPa)	2.33	0.29
Spring constant in visco-elastic phase (E_2, GPa)	2.16	0.36
Visco-plastic viscosity (η_1, GPa·day)	42.30	1.04
Visco-elastic viscosity (η_2, GPa·day)	1.35	0.10
Poisson's ratio (ν)	0.27	0.40
Shear modulus (G, GPa)	6.66	0.66
Bulk modulus (K, GPa)	12.00	3.00
Tensile strength (T, MPa)	1.88	0.23

It should be noted that the effects of $C_\%$ on the creep rate tend to be largest for the specimens with $C_\%$ between 20% and 40% where the highest magnitudes of shear stresses are concentrated. When $C_\%$ is above and below this range, the magnitudes of the localized shear stresses become lower, and hence leads to a smaller effect of the number of inter-layers. The simulation results suggest that both amount and distribution of the carnallite have a significant impact on the strength and time-dependent deformation on the rock salt specimens. They also explain the relatively high variation of the Burgers parameters for the specimens with the same $C_\%$ or the same density.
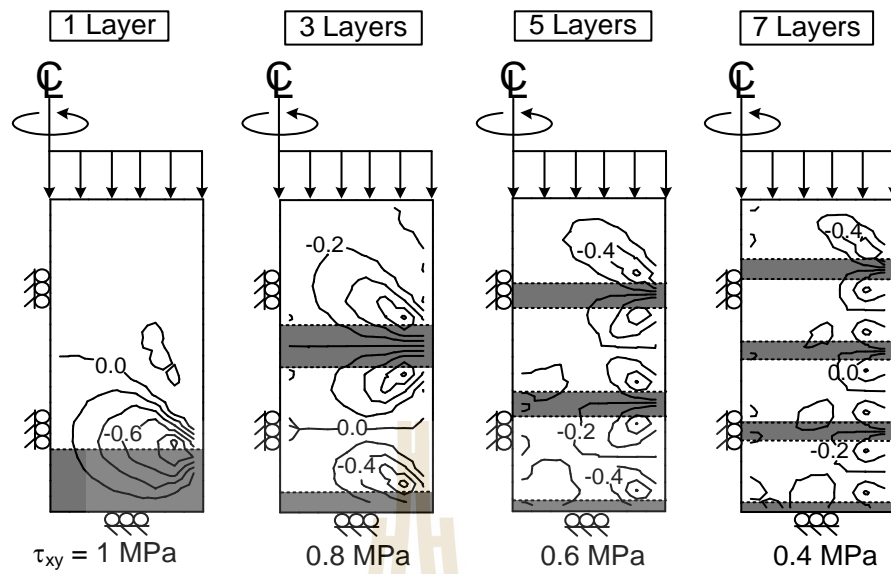
Figure 6.3 Shear stresses induced in specimens with various distributions of 20%
carnallite.
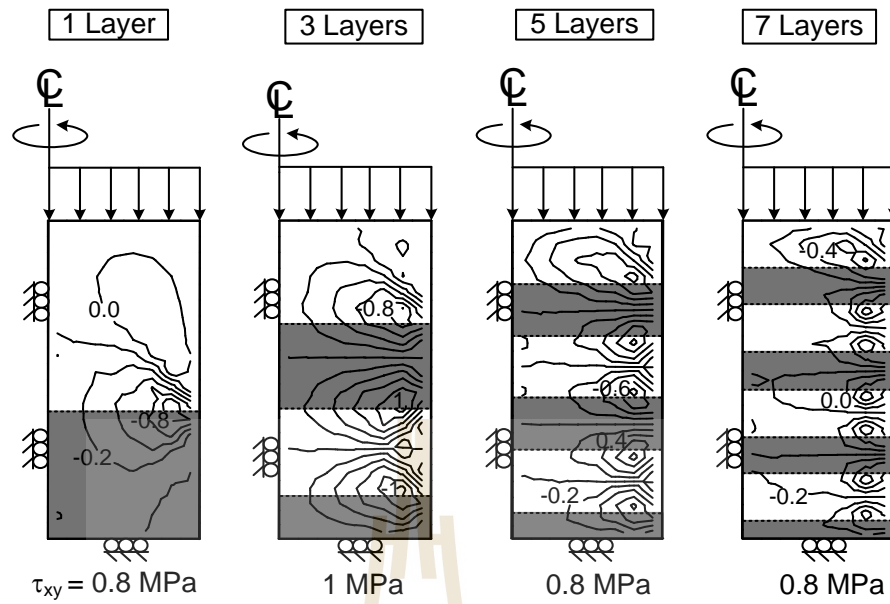
Figure 6.4 Shear stresses induced in specimens with various distributions of 40%

carnallite.
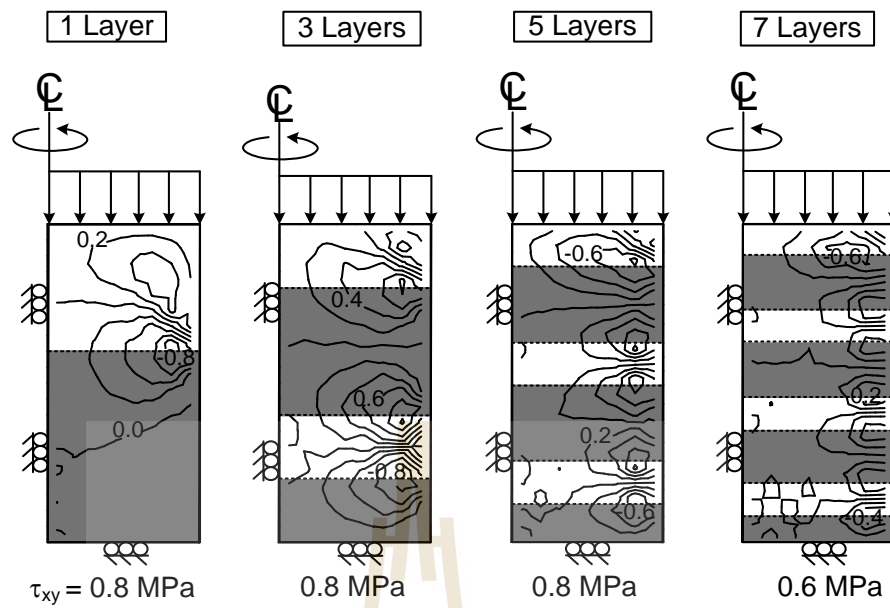
Figure 6.5 Shear stresses induced in specimens with various distributions of 60%
carnallite.
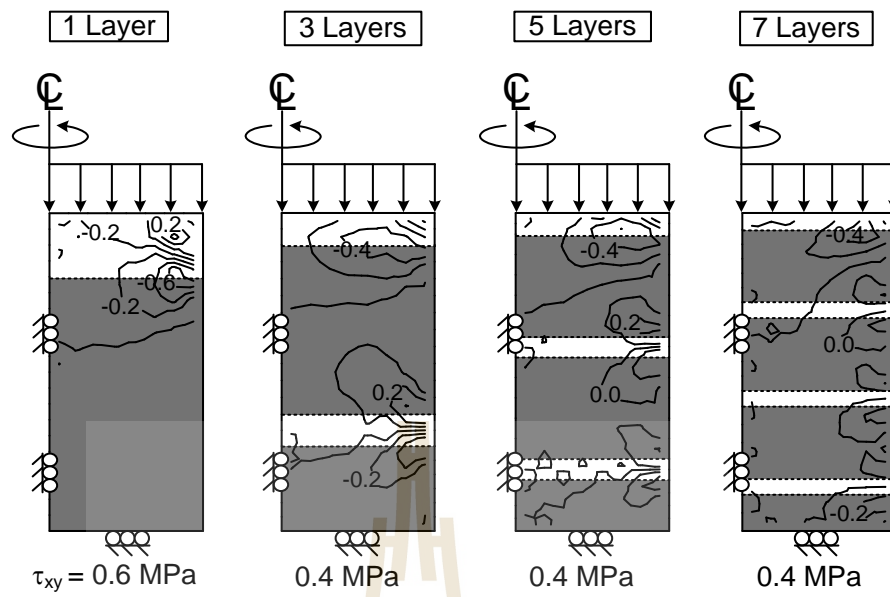
Figure 6.6 Shear stresses induced in specimens with various distributions of 80%
carnallite.
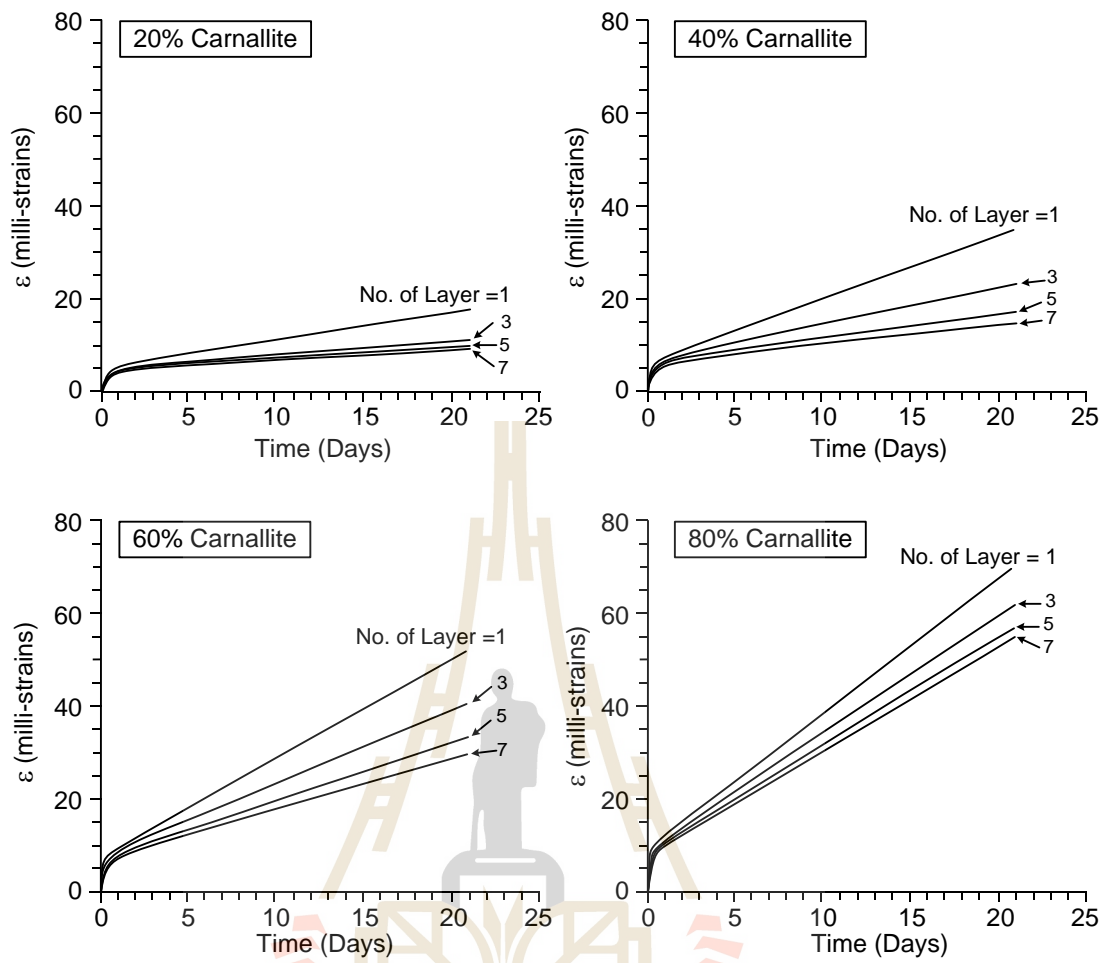
Figure 6.7 Axial strain–time curves simulated for salt specimens with $C_\%$ = 20, 40, 60 and 80%.

CHAPTER VII

BOREHOLE CLOSURE

7.1 Introduction

This chapter describes an application of creep parameters for calculation of borehole closure as affected by carnallite content. Two different creep model for use to predict borehole closure.

7.2 Creep closure from Burgers parameters

Sets of analytical solutions are derived to calculate radial displacements around shaft and borehole in an infinite of rock salt mass. The rock salt deformation is assumed to be time-independent under hydrostatic stress (i.e., linear visco-elastic material). It is recognized that the Burgers model is based on the linear visco-elastic theory. It may not truly represent the non-linear creep deformation of the in-situ rock salt around the shaft and borehole. The model is used here to demonstrate the effect of carnallite content on the rock salt creep. The radial displacement (u_r) around the cylindrical hole obtained from the elastic solution (Obert and Duvall, 1967) can be expressed as:

$$u(t) = P \cdot [\frac{1}{9K} + \frac{2}{3}\{\frac{\eta_2}{\eta_1 E_2}(\exp(-E_2 t / \eta_2) + \frac{E_2 t}{\eta_2} - 1) + (\frac{1}{E_1} + \frac{1}{E_2} + \frac{\eta_2}{E_2 \eta_1}) \cdot$$
$$(1 - \exp(-E_2 t / \eta_2)) + \frac{\exp(-E_2 t / \eta_2)}{E_1}\}](A) - P \cdot [\frac{-1}{9K} + \frac{1}{3}\{\frac{\eta_2}{\eta_1 E_2}(\exp(-E_2 t / \eta_2) + \frac{E_2 t}{\eta_2} - 1) +$$
$$(\frac{1}{E_1} + \frac{1}{E_2} + \frac{\eta_2}{E_2 \eta_1}) \cdot (1 - \exp(-E_2 t / \eta_2)) + \frac{\exp(-E_2 t / \eta_2)}{E_1}\}](B) \tag{7.1}$$

where P is a time-independent applied stress, t is time, K is bulk modulus, E_1 and E_2 are elasticity of spring, η_1 and η_2 are viscosity of dashpot, A and B are the time-independent functions of position

The hole is subjected to uniform lateral stress the functions A and B become:

$$A = r + (a^2 / r) \tag{7.2}$$

$$B = r - (a^2 / r) \tag{7.3}$$

where r is radius and a is inner boundary.

The radial displacement at the opening boundary can be determined as a function of time.

$$\varepsilon_r = u_r / 2a \tag{7.4}$$

where ε_r is radial strain.

Due to the fact that rock salt and carnallite exhibit time-dependent behavior. The behavior of rock salt and carnallite will be change approaching the failure when the time is increased. The strain energy density principle is applied here to describe the rock strength and can predict the time at the failure of rock salt and carnallite.

The distortional strain energy at dilation ($W_{d,d}$) and at failure ($W_{d,f}$) can be calculated from the shear modulus and octahedral shear stresses obtained from Luangthip et al. (2016) as follows (Jaeger et al., 2007):

$$W_{d,f} = (3/2) \cdot \tau_{oct,f} \cdot \gamma_{oct,f} \qquad (7.5)$$

$$W_{d,d} = (3/2) \cdot \tau_{oct,d} \cdot \gamma_{oct,d} \qquad (7.6)$$

where $\tau_{oct,f}$, $\tau_{oct,d}$ are octahedral shear stress at failure and at dilation, $\gamma_{oct,f}$, $\gamma_{oct,d}$ are octahedral shear strain at failre and at dilation.

The octahedral shear stress and the octahedral shear strain can be calculated as (Jaeger et al., 2007):

$$\tau_{oct} = (1/3)[(\sigma_1 - \sigma_2)^2 + (\sigma_1 - \sigma_3)^2 + (\sigma_2 - \sigma_3)^2]^{1/2} \qquad (7.7)$$

$$\gamma_{oct} = (1/3)[(\varepsilon_1 - \varepsilon_2)^2 + (\varepsilon_1 - \varepsilon_3)^2 + (\varepsilon_2 - \varepsilon_3)^2]^{1/2} \qquad (7.8)$$

where σ_1 is axial stress, σ_2 and σ_3 are lateral stresses, ε_1 is axial strain, ε_2 and ε_3 are lateral strains. The octahedral shear stress is shown in Table 7.1 and the octahedral shear strain in Table 7.2.

The diagrams (Figure 7.1) of $W_{d,d}$ and $W_{d,f}$ as a function of mean stress are constructed using text data from Luangthip et al. (2016). The strain energy criterion is used to determine the strains at failure and at dilation under the constant octahedral shear stresses induced at borehole wall for each depth. The obtained strains at failure or dilation is then compared with the strain-time curves under the some octahedral shear stress. And hence the corresponding time at failure or dilation can be predicted.

Figure 7.2 shows the strain time curves until failure and dilation with varied carnallite

contents for different depths.
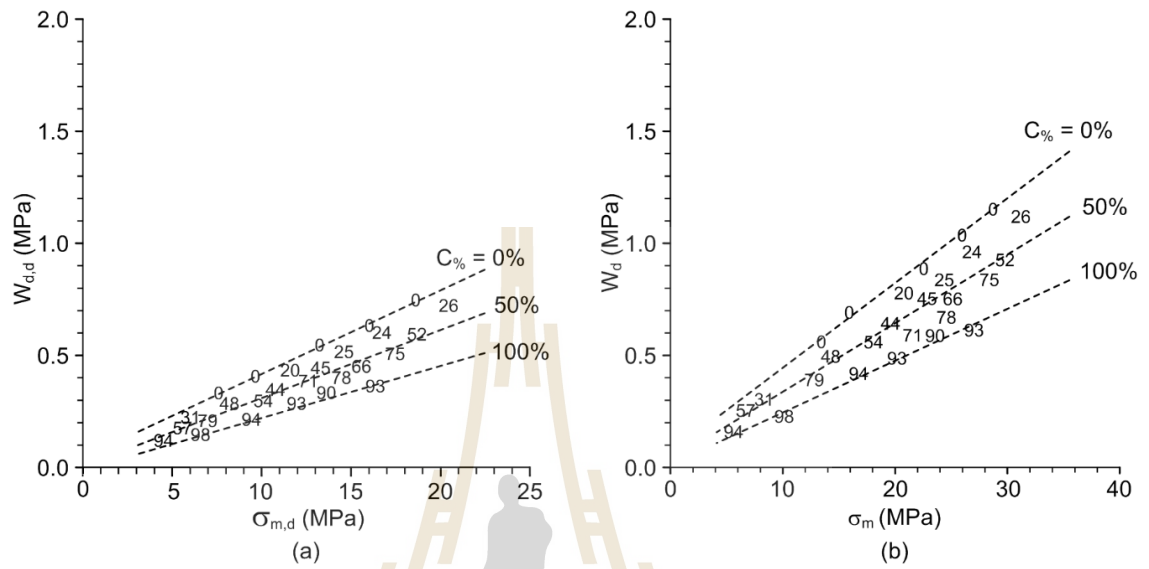
Figure 7.1 Distortional strain energy of a function of mean stress varied carnallite

contents, (a) at dilation ($W_{d,d}$) and (b) at failure ($W_{d,f}$).

Table 7.1 Summary of the octahedral shear stress and the octahedral shear strain at failure from Luangthip et al. (2016).

σ_3 (MPa)	$C_\%$	τ (MPa)	γ (MPa)	W_d (MPa)	σ_m (MPa)
	0	19.80	0.01	0.26	13.13
1.7	31	17.49	0.01	0.20	11.80
	57	15.18	0.01	0.14	10.47
	94	13.45	0.01	0.14	9.47
	0	21.94	0.01	0.36	15.67
3	48	19.05	0.01	0.28	14.00
	79	17.32	0.01	0.22	13.00
	98	12.70	0.01	0.16	10.33
	0	17.90	0.01	0.31	15.33
	20	26.56	0.01	0.43	20.33
5	44	24.25	0.01	0.35	19.00
	54	22.52	0.01	0.28	18.00
	90	20.21	0.01	0.22	16.67
	0	32.33	0.01	0.61	25.67
	25	28.87	0.01	0.51	23.67
7	45	25.98	0.01	0.44	22.00
	71	24.25	0.01	0.41	21.00
	93	21.94	0.01	0.33	19.67
	0	34.06	0.01	0.76	28.67
	24	30.60	0.01	0.65	26.67
9	66	27.14	0.01	0.54	24.67
	78	25.98	0.01	0.51	24.00
	90	24.25	0.01	0.42	23.00
	26	31.75	0.02	0.71	30.33
12	52	29.44	0.01	0.63	29.00
	75	27.71	0.01	0.59	28.00
	93	24.83	0.01	0.47	26.33

Table 7.2 Summary of the octahedral shear stress and the octahedral shear strain at dilation from Luangthip et al. (2016).

σ_3 (MPa)	$C_\%$	τ (MPa)	γ (MPa)	W_d (MPa)	σ_m (MPa)
1.7	0	12.89	0.01	0.21	9.14
	31	9.81	0.01	0.14	7.37
	57	8.47	0.01	0.11	6.59
	94	6.85	0.01	0.08	5.65
3	0	14.72	0.01	0.25	11.50
	48	12.23	0.01	0.18	10.06
	79	8.38	0.01	0.12	7.84
	98	7.56	0.01	0.10	7.36
5	0	18.43	0.01	0.34	15.64
	20	15.40	0.01	0.27	13.89
	44	13.63	0.01	0.21	12.87
	54	12.00	0.01	0.18	11.93
	90	9.68	0.01	0.13	10.59
7	0	20.40	0.01	0.39	18.78
	25	16.98	0.01	0.32	16.80
	45	15.09	0.01	0.26	15.71
	71	14.29	0.01	0.24	15.25
	93	11.26	0.01	0.17	13.50
9	0	21.95	0.01	0.46	21.68
	24	18.48	0.01	0.37	19.67
	66	14.10	0.01	0.28	17.14
	78	12.77	0.01	0.24	16.37
	90	10.90	0.01	0.20	15.29
12	26	19.44	0.01	0.43	23.23
	52	15.72	0.01	0.35	21.08
	75	13.46	0.01	0.30	19.77
	93	10.50	0.01	0.21	18.06
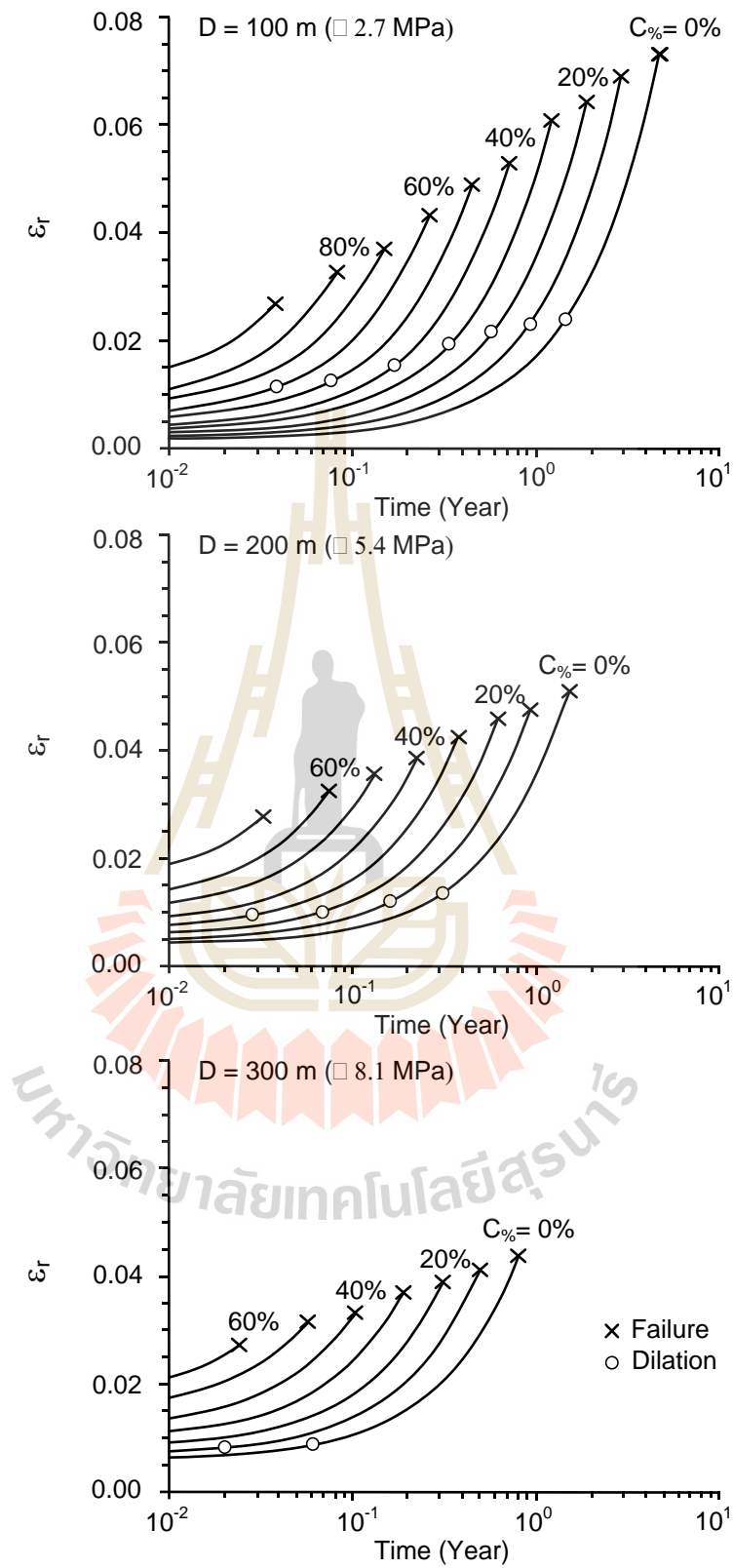
Figure 7.2 Strain time curves at failure and dilation with varied carnallite contents at

different depths: 100, 200 and 300 m (Burgers parameters).

7.3   Creep closure predicted from potential parameters

Fuenkajorn and Daemen (1988) have derived the total radial strain at radius and at time (t) which can be presented as:

$$\varepsilon_r(t) = \frac{1}{E}\left\{(1-\nu^2)\sigma_r - \nu(1+\nu)\sigma_\theta\right\} + \frac{3}{2}\kappa(\sigma^*)^{(\beta-1)} \cdot S_r t^\gamma \tag{7.9}$$

where κ, β and γ are material constants of the potential creep law, S_r is the radial stress deviation, and σ^* is the equivalent (effective) stress. The stress deviation can be obtained from:

$$S_r = \sigma_r - (\sigma_r + \sigma_\theta + \sigma_z)/3 \tag{7.10}$$

Based on the von Mises flow rule σ^* is defined as:

$$\sigma^* = \frac{1}{\sqrt{2}}\left\{(\sigma_r-\sigma_\theta)^2 + (\sigma_\theta-\sigma_z)^2 + (\sigma_z-\sigma_r)^2\right\}^{\frac{1}{2}} \tag{7.11}$$

The stress distributions around circular borehole can be calculated under plane strain condition by using the Kirsch's solution (Brady and Brown, 2006). The radial (σ_r) tangential (σ_θ) and vertical (σ_z) stresses can be calculated by (Jaeger et al., 2007):

$$\sigma_r = (1-\frac{a^2}{r^2})P_o + P_i(\frac{a^2}{r^2}) \tag{7.12}$$

$$\sigma_\theta = (1+\frac{a^2}{r^2})P_o - P_i(\frac{a^2}{r^2}) \tag{7.13}$$

where a is borehole radius, r is radial distance from the center, P_o and P_i are constant external and internal pressures. Here P_i is assumed here to be zero. Under plane strain condition the axial stress (σ_z) can be determined by:

$$\sigma_z = \nu \cdot (\sigma_r + \sigma_\theta) \tag{7.14}$$

For this demonstration P_o is ranged from 2.7, 5.4 to 8.1 MPa. They are equivalent to the depths approximately of 100, 200, and 300 m, respectively. The calculation of the strain energy criteria from Equation (7.5) and Equation (7.6), by using the same method as those of the Burgers model.

The strength criterion derived earlier is applied to determine the stability of rock salt around borehole subjected to uniform external pressures. This is primarily to demonstrate the potential application of the strength criterion that has been derived from test data under different C% values. Figure 7.3 shows the strain time curves at failure and dilation with varied carnallite contents at different depths. The result shows that the time at failure decreases when carnallite content is increasing.

67
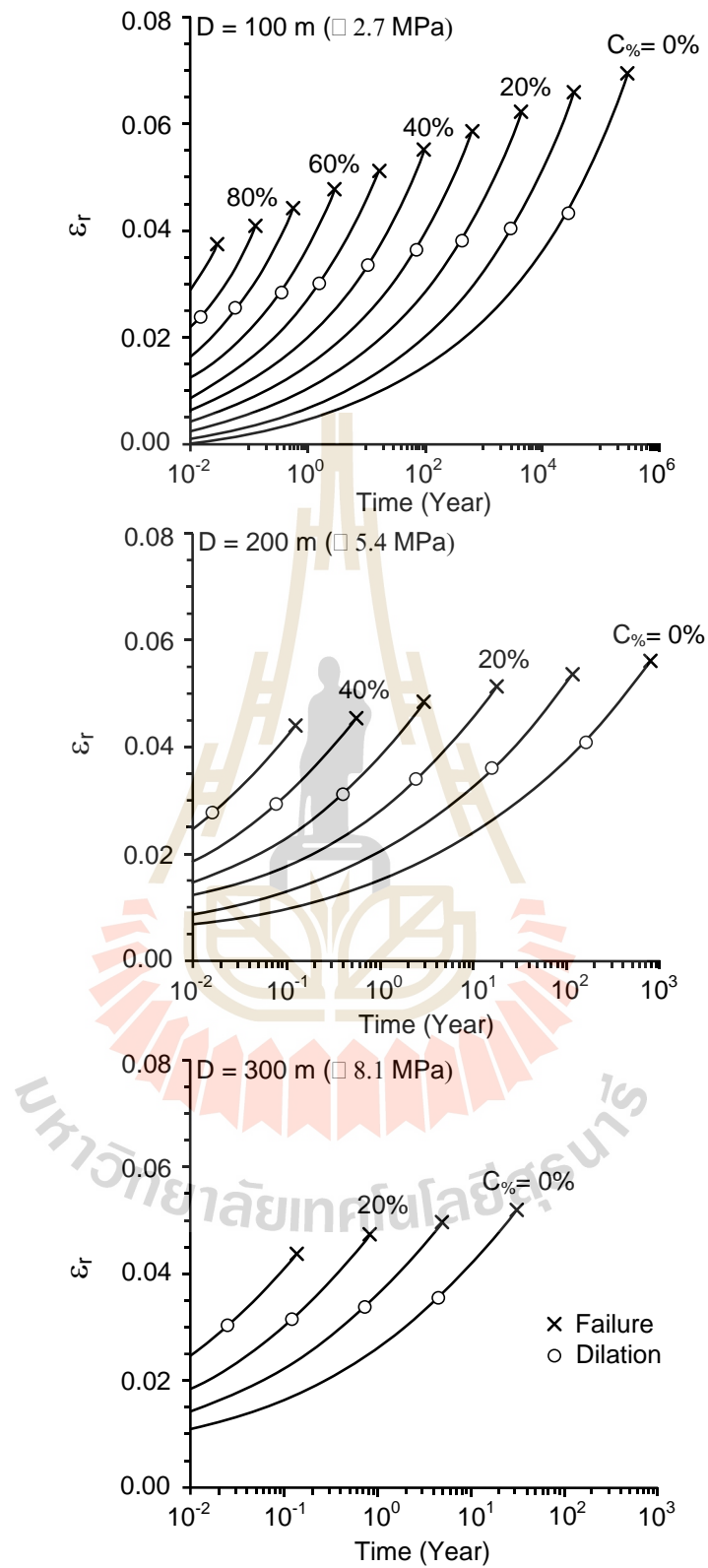
Figure 7.3 Strain time curves at failure and dilation with varied carnallite contents at

different depths: 100, 200 and 300 m (potential parameters).

CHAPTER VIII

DISCUSSIONS, CONCLUSIONS AND

RECOMMENDATIONS FOR FUTURE STUDIES

8.1 Discussions

This section discusses the key issues relevant to the reliability of the test schemes and the adequacies of the test results. The objective of this research is to experimentally determine the effects of carnallite contents on the instantaneous and time-dependent deformations of rock salt. This thesis describes the detailed test methods, the derivation of the visco-elastic governing equation, and the predict deformation of rock salt with varied carnallite content.

- The numbers of the test specimens seem adequate, as evidenced by the good coefficients of correlation for all uniaxial and triaxial creep test.

- The Burgers model is used to describe the time-dependent deformation of the creep test specimens. It is recognized that numerous creep models or constitutive equations have been developed to represent the time-dependent behavior of rock salt (e.g., Gnirk and Johnson 1964; Handin et al. 1984; Langer 1984; Hardy and Sun 1986; Senseny et al. 1983). The Burgers model is used because it is simple and capable of describing the elastic, visco-elastic and visco-plastic phases of deformation.

- Burgers model and potential law can adequately represent the creep behavior of the specimens under various carnallite contents.

- The advantage of the application of the stain energy criterion over the octahedral shear-mean stress criterion is that it considers both stress and strain at failure.

8.2 Conclusions

All objectives and requirements of this study have been met. The results of the laboratory testing and analyses can be concluded as follows:

- The effect of carnallite content can be observed from the increase of the axial strain as the carnallite increases, as shown in Figure 4.3. The creep deformation for the pure halite specimens agrees well with those of (Fuenkajorn, 2007) who performs creep testing on the same salt. This is due to the fact that the rock salt with carnallite contents are softer and can flow more easily than does the rock salt with pure halite.

- The effects of $C_\%$ on the creep rate tend to be largest for the specimens with $C_\%$ between 20% and 40%. When $C_\%$ is above and below this range, the magnitudes of the localized shear stresses become lower, and hence leads to a smaller effect of the number of inter-layers. The simulation results suggest that both amount and distribution of the carnallite have a significant impact on the strength and time-dependent deformation of the rock salt specimens.

- The strain energy criterion is used to determine the strains at failure and at dilation under the constant octahedral shear stresses induced at borehole wall for each depth. The result indicate that the time at failure and dilation decreases as the carnallite content increases.

8.3   Recommendations for future studies

- Some uncertainties of the investigation and results discussed above lead to the recommendations for further studies. More testing is required on a variety of specimen with different of carnallite content. Determine contamination of carnallite content by density may be inaccurate. Methods to determine the carnallite content inclusions should be developed for a more precisely determination.

- The constitutive law used in this study may not adequately describe the salt behavior. Other constitutive laws, such as liner visco-plastic and exponential law may be needed to describe the salt behavior. Should be tested under different temperatures to study the behavior of rock salt and carnallite.
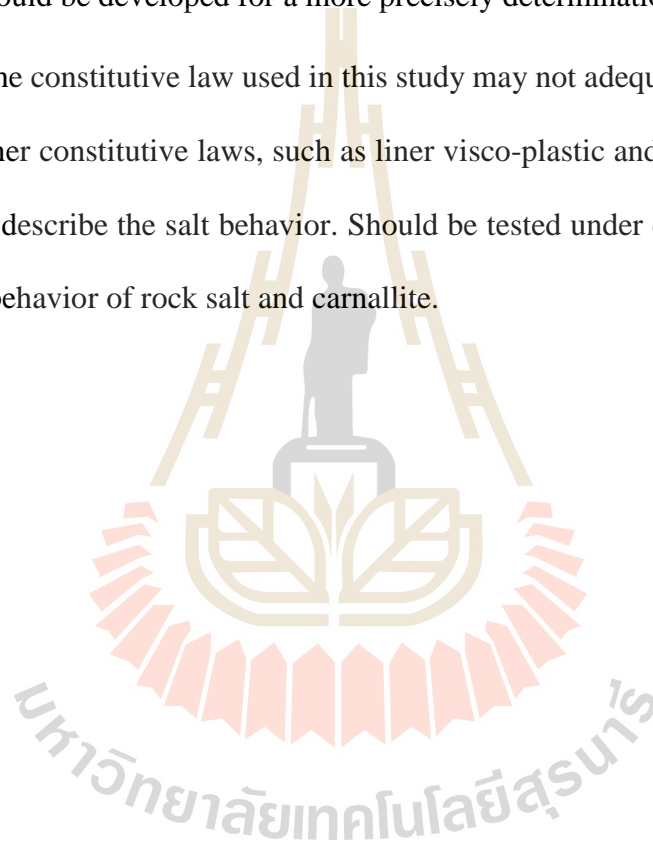
REFERENCES

Allemandou, X. and Dusseault, M. B. (1996). Procedures for cyclic creep testing of salt rock, results and discussions. In **Proceedings of the Third Conference on the Mechanical Behavior of Salt** (pp. 207-218). Clausthal-Zellerfeld: Trans Tech Publications.

ASTM D2664-95a. Standard test method for triaxial compressive strength of undrained rock core specimens without pore pressure measurements. In **Annual Book of ASTM Standards** (Vol. 04.08). Philadelphia: American Society for Testing and Materials.

ASTM D2938-95. Standard test method for unconfined compressive strength of intact rock core specimens. In **Annual Book of ASTM Standards** (Vol. 04.08). Philadelphia: American Society for Testing and Materials. 69

ASTM D3967-95a. Standard test method for splitting tensile strength of intact rock core specimens. In **Annual Book of ASTM Standards** (Vol. 04.08). Philadelphia: American Society for Testing and Materials.

ASTM Standard D7070-08, 2008, Standard test methods for creep of rock core under constant stress and temperature. **Annual Book of ASTM Standards**, American Society for Testing and Materials, West Conshohocken, P.A., Vol. 04.09.

Aubertin, M., Julien M. R., Servant, S. and Gill, D. E. (1999). A rate-dependent model for the ductile behavior of salt rocks. **Canadian Geotechnical Journal**. 36(4): 660-674.

Aubertin, M., Sgaoula, J. and Gill, D. E. (1992). A damage model for rock salt: Application to tertiary creep. In **The Seventh Symposuim on Salt** (pp. 117-125). Elsevier Science Pub.

Aubertin, M., Sgaoula, J. and Gill, D. E. (1993). Constitutive modeling of rock salt: Basic considerations for semi-brittle behavior. In **Proceedings of the Fourth International Symposuim on Plasticity and It's Current Applications** (pp. 92). Baltimore.

Aubertin, M., Sgaoulla, J., Servant, S., Julien, M. R., Gill, D. E. and Ladanyi, B. (1998). An upto-date version of SUVIC-D for modeling the behavior of salt. In **Proceedings of the Fourth Conference on the Mechanical Behavior of Salt** (pp. 205-220). Clausthal, Germany: Trans Tech Publications.

Bachu, S. and Dusseault, M. B. (2005). Underground injection of carbon dioxide in salt beds. **Developments in Water Science** 52: 637-648.

Berest, P., Brouard, B. and Durup, J. G. (2000). Shut-in pressure test: Case studies. In **Proceedings Solution Mining Research Institute 2000 Fall Technical Meeting**, San Antonio, TX.

Brady, B.H.G. and Brown, E.T. (2006). Rock Mechanics for Underground Mining. **Third ed. Springer**, Netherlands.

Chen, H, Evitts, R.W. and Besant, R.W. (2006). Moisture adsorption characteristics of a thin bed of polycrystalline potash pellets Part II Modeling and numerical simulation. **Powder technology.** 171: 46-53.

Chokski, A. H. and Langdon, T. G. (1991). Characteristics of creep deformation in ceramics. **Materails Science and Technology**. 7: 577-584.

Duncan, E.J.S. and Lajtai, E. (1993). The creep of potash salt rocks from Saskatchewan. **Geotechnical and Geological engineering.** 11: 159-184.

Dusseault, M.B. and Fordham, C.J. (1993). Time-dependent behavior of rocks. **Comprehensive Rock Engineering Principles, Practice and Project: Rock Testing and Site Characterization** (Vol. 3, pp.119-149). London, Pergamon.

Fahimifar, A., Tehrani, F.M., Hedavat, A. and Vakilzadeh. (2010). Analytical solution for the excavation of circular tunnels in a visco-elastic Burger's material under hydrostatic stress field. **Tunneling and Underground Space Technology.** 25(4): 297-304.

Farmer, I.W. (1983). Engineering Behavior of Rock. **2nd edition**, Chapman and Hall, Ltd., New York.

Fokker, P. A. (1995). The behavior of salt and salt caverns. **Ph.D Thesis**, Delft University of Technolgoy.

Fokker, P. A. (1998). The micro-mechanics of creep in rock salt. In **Proceedings of the Fourth Conference on the Mechanical Behavior of Salt** (pp. 49-61). Clausthal-Zellerfeld, Germany: Trans Tech Publications.

Fokker, P. A. and Kenter, C. J. (1994). The micro mechanical description of rock salt plasticity. **In Eurock'94** (pp. 705-713). Rotterdam: Balkema.

Franssen, R.C.M. and Spiers, C.J. (1990). Deformation of polycrystalline salt in compression and in shear at 250-350°C, In: KNIPE, R. J. and RUTTER, E.H. (eds) Deformation Mechanisms, Rheology and Tectonics. **Geological Society Special Publication**. 54: 201-213.

Fuenkajorn, K. and Daemen, J. J. K. (1988). Boreholes closure in salt. **Technical Report Prepared for The U.S. Nuclear Regulatory Commission.** Report No. NUREG/CR-5243 RW. University of Arizona.

Fuenkajorn, K. (2007). Intrinsic variability of the mechanical properties of Maha Sarakham salt**. International Journal of Rock Mechanics and Mining Sciences.** 15(1): 33-48.

Fuenkajorn, K. and Phueakphum, D. (2010). Effects of cyclic loading on mechanical properties of Maha Sarakham salt. **Engineering Geology**. 112 (1-4) 43-52.

Fuenkajorn, K. and Serata, S. (1994). Dilationinduced permeability increase around caverns in rock salt. **Proceeding of the 1st North American Rock Mechanics Symposium** (p. 648-656); June 1-3, Rotterdam: A.A. Balkema.

Fuenkajorn, K., Sriapai, T. and Samsri, P. (2012). Effects of loading rate on strength and deformability of Maha Sarakham salt. **Engineering Geology** 135-136: 10-23.

Gnirk, P.F., Johnson, R.E. (1964). The deformational behavior of a circular mine shaft situated in a viscoelastic medium under hydrostatic stress. **Proceedings of the 6th U.S. Symposium on Rock Mechanics** (pp. 233-259), University of Missouri, Rolla.

Hamami, M., Tijani, S. M. and Vouille, G. (1996). A methodology for the identification of rock salt behavior using multi-step creep tests. In **Proceedings of the Third Conference on the Mechanical Behavior of Salt** (pp. 53-66). Clausthal, Germany: Trans Tech Publications.

Handin, J., Russell, J.E. and Carter, N.L. (1984). Transient Creep of Repository Rocks. Final Report: **Mechanistic Creep Laws for Rock Salts**, Texas A & M research

Foundation, Office of Nuclear Waste Isolation, Battelled Memorial Institute, Report, BMI/ONWI-550.

Hardy, H.R. and Sun, X. (1986). A nonlinear rheological model for time-dependent behavior of geologic materials. **Proceeding of 27th U.S. Symposium on Rock Mechanics (**pp. 205-212), University of Albama, Tuscaloosa, June 23-25, Howard L, Hartman ed., Ch. 2.

Harrington, T.J. (1980). Time-Dependent Closure Analysis of a Nuclear Waste Repository in Bedded Salt. **Proceedings of the 21st U.S. Symposium on Rock Mechanics (**pp. 26-34), University of Missouri, Rolla, May 28-30, 1980, D.A. Summers, ed., published by the University of Missouri, Rolla.

Hawthorne, F.C. and Ferguson, R.B. (1975). Anhydrous sulphates. II. Refinement of the crystal structure of anhydrite. **Canadian Mineralogist.** 13:289-292.

Horseman, S. and Passaris,E. (1984). Creep Tests for Storage Cavity Closure Prediction, Mechanical Behavior of Salt I. **Proceedings of the First Conference on the Mechanical Behavior of Salt** (pp. 119-157), The Pennsylvania State University, November 9-11, 1981, Trans Tech Publications, Clausthal-Zellerfeld, Federal Republic of Germany.

Itasca (1992). **User manual for FLAC-Fast Langrangian Analysis of Continua, Version 3.0.** Itasca Consulting Group Inc., Minnespolis, MN.

Itasca (1992a). **FLAC-Fast Langrangian Analysis of Continua, Version 4.0, User Manual.** Itasca Consulting Group Inc., Minnespolis, MN, USA.

Itasca (1992b). **User manual for FLAC-Fast Langrangian Analysis of Continua, Version 4.0, User Manual.** Itasca Consulting Group Inc., Minnespolis, MN, USA.

Jaeger, J. C., Cook, N. G. W. and Zimmerman, R.W. (2007). **Fundamentals of Rock Mechanics Fourth Edition** (500 pp.). Blackwell publishing, Oxford.

Jandakaew, M. (2003). Experimental assessment of stress path effects on rock salt deformation, [M.Sc. thesis]. School of Geotechnology. **Institute of Engineering, Suranaree University of Technology.** Thailand. 139p.

Jandakaew, M. (2007). Stress-path dependency of rock salt. In **Proc of First Thailand Symposium on Rock Mechanics** (pp. 171-188), September, 13-14, Greenery Resort, Khao Yai, Nakhon Ratchasima, Suranaree University of Technology.

Jeremic, M. L. (1994). Rock mechanics in salt mining. **Rotherdam**: A. A. Balkema. 530 p.

King, M.S. (1972). Creep in model pillars of Saskatchewan potash. **International Journal of Rock Mechanics and Mining Sciences.** 10: 363-371.

Klein, C., Hurlbut, C.S. and Dana, J.D. (1988). **Manual of Mineralogy**. John Wiley and Sons Inc. Wiley, New York. 571p.

Knowles, M. K., Borns, D., Fredrich, J., Holcomb, D., Price, R. and Zeuch, D. (1998). Testing the disturbed zone aroud a rigid inclusion in salt. In **Proceedings of the Fourth Conference on the Mechanical Behavior of Salt** (pp. 175-188). Clausthal, Germany: Trans Tech Publications.

Korthaus, E. (1996). Measurement of crushed salt consolidation under hydrostatic and deviatoric stress conditions. In **Proceedings of the Third Conference on the Mechanical Behavior of Salt** (pp. 311-322). Clausthal, Germany: Trans Tech Publications.

Langer, M. (1984). The Rheologial Behaviour of Rock Salt, Mechanical Behavior of Salt I. **Proceedings of the First Conference on the Mechanical Behavior of**

Salt (pp. 201-240). The Pennsylvania State University, November 9-11, 1981, Trans Tech Publications, ClausthalZellerfeld, Federal Republic of Germany.

Lindner, E.N. and B.H.G. Blrady. (1984). Memory Aspects of Salt Creep, Mechanical Behavior of Salt I. **Proceedings of the First Conference on the Mechanica Behavior of Salt** (pp. 241-273). The Pennsylvania State University, November 9-11, 1981, Trans Tech Publications, Clausthal-Zellerfeld, Federal Republic of Germany.

Luangthip, A., Khamrat, S. and Fuenkajorn, K. (2016). Effects of Carnallite Contents on Stability and Extraction Ratio of Potash Mine. In **9th Asian Rock Mechanics Symposium**. October 18-20, Bali, Indonesia.

Mellegard, K. D., Robert, L. A., and Callahan, G. D. (2012). Effect of sylvite content on mechanical properties of potash. **Mechanical Behavior of Salt VII-Berest, Ghoreychi, Hadj-Hassen and Tijani** (pp. 71-79). Taylor and Francis Group, London.

Munson, D. E. and Wawersik, W. R. (1993). Constitutive modeling of salt behavior – State of the technology. In **Proceedings of the Seventh International Congess on Rock Mechanics** (vol. 3, pp. 1797-1810). Balkema.

Munteanu, L.P. and Cristescu, N.D. (2000). Stress relaxation during creep of rocks around deep boreholes. **International Journal of Engineering Science**. 39(7): 737-754.

Nair, K. and Boresi, A.P. (1970). Stress Analysis for Time Dependent Problems in Rock Mechanics. **Proceedings 2nd Congress of the International Society for Rock Mechanics** (pp. 531-536), Belgrade, 2(4).

Nair, K., Chang, C.Y., Singh, R.D. and Abdullah, A.M. (1974). Time-Dependent Analysis to Predict Closure in Salt Cavities. **Proceedings of the Fourth Symposium on Salt** (pp. 129-139), Vol. 2, A.H. Coogan, ed., The Northern Ohio Geological Society, Inc., Cleveland, Ohio.

Obert, L. and Duvall, W.I. (1967). Rock mechanics and the design of structures in rock. **Journal of the Franklin Institute**, New York.

Ong, V., Unrau, J., Jones, J. Coode, A. and Mackintosh, D. (1998). Triaxial creep testing of saskatchewan potash samples. In **Proceedings of the Fourth Conference on the Mechanical Behavior of Salt** (pp. 469-480). Clausthal, Germany: Trans Tech Publications.

Raj, S.V. and Pharr, G.M. (1992). Effect of temperature on the formation of creep substructure in sodium chloride single crystal. **American Ceramic Society**. 75(2): 347-352.

Richard, J. (1993). Plasticity and Creep. Theory, Example, and Problems, English Edition Editor, **Rochester Institute of Technology**, Rochester, New York.

Schlemper, E.O., Sen Gupta, P.K. and zoltai, T. (1985). Refinement of the structure of carnallite, $Mg \cdot (H_2O)_6 KCl_3$. **American Mineralogist**. 70(11-12): 1309-1313.

Senseny, P. E. (1984). Specimen size and history effects on creep of salt. In **Proceedings of the First Conference on the Mechanics Behavior of Salt** (pp. 369-379). Clausthal-Zellerfeld: Trans Tech Publications.

Senseny, P.E., Handin, J.W., Hansen, F.D., and Russell, J.E. (1992). Mechanical behavior of rock salt: phenomenology and micromechanisms. **Int J Rock Mech Min Sci**. 29(4):363-37.

Shen, Zhenzhong, Xu, Zhiying, 1997. Creep test of granite for the three gorges dam foundation. **Journal of Hohai University** 2, 1–7 (in Chinese).

Sriapai, T., Walsri, C., and Fuenkajorn, K. (2012). Effect of temperature on compressive and tensile strength of salt. **ScienceAsia.** 38: 166-174.

Starfield, A.M. and McClain, W.C. (1973). Project Salt Vault: A Case Study in Rock Mechanics. **International Journal of Rock Mechanics and Mining Sciences & Geomechanics Abstracts**, Pergamon Press, Great Britain. 10(6): 641-657.

Stormont, J.C. and Fuenkajorn, K. (1994). Dilation-induced permeability changes in rock salt. **Proceedings of the 8th International Conference on Computer Methods and Advances in Geomechanics** (pp. 1,296-1,273); May 1994; Morgantown, West Virginia, USA.

Suwanich, P. (2007). Potash-evaporite deposits in Thailand. In **Proceedings of the International Conference on Geology of Thailand** (pp. 252-262). 21-22 November 2007, Department of Mineral Resources, Thailand.

Wang, Z. and Li, Y. (2007). Rock Rheological Theory and Numerical Simulation. **Science Press**, Beijing (in Chinese).

Warren, J. 1999. Evaporites: Their Evolution and Economics, **Blackwell Science**, Oxford.

Weck, P.F., Kim, E., Jové-Colón, C.F. and Sassani, D.C. (2014). First-principles study of anhydrite, polyhalite and carnallite. **Chemical Physics Letters**. 594: 1-5.

Weidinger, P., Hampel, A., Blum, W. and Hunsche, U. (1997). Creep behavior of natural rock salt and its description with the composite model. **Materials Science and Engineering.** 646-648.

Wendai, L. 2000. Regression analysis, linear regression and probit regression, in 13 chapters, SPSS for Windows: statistical analysis: Publishing House of Electronics Industry, Beijing.

Wetchasat, K. (2002). Assessment of mechanical performance of rock salt formations for nuclear waste repository in northeastern Thailand, [M.Sc. thesis]. **School of Geotechnology.** Suranaree University of Technology. Thailand. 179p.

Yahya, O.M.L., Aubertin, M. and Julien, M.R. (2000). A unified representation of the plasticity, creep and relaxation behavior of rock salt. **International Journal of Rock Mechanics and Mining Sciences.** 37:787-800.

Yang, C., Daemen, J.J.K. and Yin, J.H. (1999). Experimental investigation of creep behavior of salt rock. **International Journal of Rock Mechanics and Mining Sciences.** 36: 233-242.

Zhang, H., Wang, Z., Zheng, Y., Duan, P. and Ding, S. (2012). Study on tri-axial creep experiment and constitutive relation of different rock salt. **Safety science.** 50:801-805.

BIOGRAPHY

Miss Naphaphat Wilalk was born on April 18, 1993 in Chachoengsao, Thailand. She received her Bachelor's Degree in Engineering (Geotechnology) from Suranaree University of Technology in 2015. For her post-graduate, she continued to study with a Master's degree in the Geological Engineering Program, Institute of Engineering, Suranaree university of Technology. During graduation, 2015-2017, she was a part time worker in position of research assistant at the Geomechanics Research Unit, Institute of Engineering, Suranaree University of Technology.